Diverse rupture modes for surface-deforming upper plate earthquakes in the southern Puget Lowland of Washington State

Alan R. Nelson[1,*], Stephen F. Personius[1], Brian L. Sherrod[2], Harvey M. Kelsey[3], Samuel Y. Johnson[4], Lee-Ann Bradley[1], and Ray E. Wells[5]

[1]*Geologic Hazards Science Center, U.S. Geological Survey, MS 966, PO Box 25046, Denver, Colorado 80225, USA*

[2]*U.S. Geological Survey at Department of Earth and Space Sciences, University of Washington, Box 351310, Seattle, Washington 98195, USA*

[3]*Department of Geology, Humboldt State University, Arcata, California 95521, USA*

[4]*Western Coastal and Marine Geology Science Center, U.S. Geological Survey, 400 Natural Bridges Drive, Santa Cruz, California 95060, USA*

[5]*Geology, Minerals, Energy, and Geophysics Science Center, U.S. Geological Survey, 345 Middlefield Road, MS 973, Menlo Park, California 94025, USA*

ABSTRACT

Earthquake prehistory of the southern Puget Lowland, in the north-south compressive regime of the migrating Cascadia forearc, reflects diverse earthquake rupture modes with variable recurrence. Stratigraphy and Bayesian analyses of previously reported and new ^{14}C ages in trenches and cores along backthrust scarps in the Seattle fault zone restrict a large earthquake to 1040–910 cal yr B.P. (2σ), an interval that includes the time of the M 7–7.5 Restoration Point earthquake. A newly identified surface-rupturing earthquake along the Waterman Point backthrust dates to 940–380 cal yr B.P., bringing the number of earthquakes in the Seattle fault zone in the past 3500 yr to 4 or 5. Whether scarps record earthquakes of moderate (M 5.5–6.0) or large (M 6.5–7.0) magnitude, backthrusts of the Seattle fault zone may slip during moderate to large earthquakes every few hundred years for periods of 1000–2000 yr, and then not slip for periods of at least several thousands of years. Four new fault scarp trenches in the Tacoma fault zone show evidence of late Holocene folding and faulting about the time of a large earthquake or earthquakes inferred from widespread coseismic subsidence ca. 1000 cal yr B.P.; 12 ages from 8 sites in the Tacoma fault zone limit the earthquakes to 1050–980 cal yr B.P. Evidence is too sparse to determine whether a large earthquake was closely predated or postdated by other earthquakes in the Tacoma basin, but the scarp of the Tacoma fault was formed by multiple earthquakes. In the northeast-striking Saddle Mountain deformation zone, along the western limit of the Seattle and Tacoma fault zones, analysis of previous ages limits earthquakes to 1200–310 cal yr B.P. The prehistory clarifies earthquake clustering in the central Puget Lowland, but cannot resolve potential structural links among the three Holocene fault zones.

INTRODUCTION

The seismic hazard of active convergent margins derives not only from great earthquakes on the megathrust, but also from shallow faulting in the actively deforming forearc. Along the Cascadia margin, the cities of Seattle and Tacoma occupy the Puget Lowland, a structurally complex, seismically active forearc trough between the Coast Range and the Cascade volcanic arc. Deformation of the lowland is caused by the clockwise motion of western Oregon, pushing northward and compressing western Washington against slower moving Canada (Fig. 1A; Wells and Simpson, 2001; McCaffrey et al., 2007). North-south shortening of the Puget Lowland at ~4.4 mm/yr (McCaffrey et al., 2007) has produced thrust fault–bounded uplifts that subdivide the lowland into four basins (Fig. 1B; Pratt et al., 1997; Brocher et al., 2001; Blakely et al., 2002). Much of the north- to northeast-directed strain in the southern Puget Lowland is accommodated by deformation in the Seattle fault zone, the Tacoma fault zone, the Saddle Mountain deformation zone, and along the Olympia fault (Figs. 1B, 1C).

The Puget Lowland tectonic setting is similar to that of southwest Japan, where the westward-migrating forearc has deformed the Seto Inland Sea into a series of basins and uplifts bounded by faults. One of these, the Nojima fault, produced the 1995 M_w6.9 Hyogoken Nanbu (Kobe) earthquake, which killed more than 6400 people, destroyed the port of Kobe, and caused $100 billion in damage (Chang, 2010). Unlike the Inland Sea of Japan, the historical record of seismicity in the Puget Lowland is short, and information about past large, surface-deforming earthquakes must come from paleoseismology. In this densely forested, heavily glaciated region, the most successful paleoseismology studies begin with aeromagnetic mapping and seismic reflection surveys to identify potentially active fault zones, move to searches for fault or fold scarps and deformed shorelines on lidar (light detection and ranging; i.e., airborne laser swath mapping) imagery, and follow up with studies of Holocene stratigraphy beneath scarps and shorelines to date prehistoric earthquake deformation (Barnett et al., 2010; e.g., Blakely et al., 2002; Johnson et al., 2004a; Sherrod et al., 2004a, 2008; Kelsey et al., 2012).

Paleoseismology has uncovered several aspects of fault and earthquake behavior in the Seattle-Tacoma-Saddle Mountain fault systems.

1. A very large earthquake is recorded by an uplifted marine terrace first identified at Restoration Point on Bainbridge Island (Fig. 2A). The terrace, uplifted during an earthquake on the master-ramp thrust of the Seattle fault, can be traced over tens of square kilometers on the fault hanging-wall block (Bucknam et al., 1992; Sherrod et al., 2000; Kelsey et al., 2008; Figs. 2A and 3).

2. Surface-rupturing reverse faults are well documented in the hanging-wall blocks of the

*Email: anelson@usgs.gov

Geosphere; August 2014; v. 10; no. 4; p. 769–796; doi:10.1130/GES00967.1; 14 figures; 1 table; 1 supplemental file.
Received 22 July 2013 ♦ Revision received 24 February 2014 ♦ Accepted 3 June 2014 ♦ Published online 24 June 2014

Seattle and Tacoma faults, as well as along faults of the Saddle Mountain deformation zone (Fig. 1C; Witter et al., 2008; Blakely et al., 2009; this paper). In the central Seattle fault zone, the surface ruptures are on short, en echelon backthrusts (Nelson et al., 2003a), and their relation to slip on the master thrust at depth is problematic (Kelsey et al., 2008).

3. Widespread evidence for surface-deforming earthquakes within ~100–200 yr of 1000 cal yr B.P. extends over at least 800 km^2 (Bucknam et al., 1992; Sherrod, 2001) and probably >4000 km^2 (Blakely et al., 2009; Martin and Bourgeois, 2012) of the southern Puget Lowland. This includes the Seattle fault zone, the Tacoma fault zone and Tacoma basin, and the Saddle Mountain deformation zone (Fig. 1C; Atwater and Moore, 1992; Bucknam et al., 1992; Bucknam and Biasi, 1994; Atwater, 1999; Sherrod et al., 2000; Hughes, 2005; Kelsey et al., 2008; Blakely et al., 2009; Arcos, 2012).

4. Apparent quiescent intervals of 6000–8000 yr have been inferred for 2 faults marked by short scarps of the central Seattle fault zone (Nelson et al., 2003a; this paper). The significance of the apparent clustering of earthquakes on these faults in the late Holocene is unclear, partly because the structural relation of the faults to the master-ramp thrust is not understood.

In this paper we reconstruct the prehistory of large earthquakes in the southern Puget Lowland (Fig. 1B). Our objectives are to interpret new and previously published evidence for surface-deforming earthquakes above the master-ramp thrusts of the Seattle and Tacoma faults, to compare earthquake chronologies among sites, and to assess the timing of large earthquakes on these faults and the kinematically related Saddle Mountain deformation zone. To do this, we describe, date, and interpret new evidence of surface-deforming earthquakes in nine fault scarp trenches in the Seattle and Tacoma fault zones (Nelson et al., 2003b, 2008; Sherrod et al., 2004a) and from wetland stratigraphy adjacent to one of the trenched scarps in the Seattle fault zone. We synthesize these new interpretations with prior studies of uplifted, subsided, or warped shorelines (Bucknam et al., 1992; Sherrod et al., 2000; Sherrod, 2001; Kelsey et al., 2008; Arcos, 2012), fault scarp and fold scarp stratigraphy (Nelson et al., 2002, 2003a; Witter et al., 2008; Blakely et al., 2009), wetland stratigraphy adjacent to scarps (Hughes, 2005; Polenz et al., 2011), strong-shaking–induced liquefaction and landslide deposits (Fig. 1C; Karlin and Abella, 1992, 1996; Pringle et al., 1998; Sherrod, 2001; Karlin et al., 2004; Martin and Bourgeois, 2012; Arcos, 2012), and the deposits of tsunamis generated by fault rupture (Atwater and Moore, 1992; Bourgeois and Johnson, 2001; Arcos, 2012; Martin and Bourgeois, 2012). A key part of our synthesis is an evaluation of the more than 260 ^{14}C ages obtained during paleoseismic studies in the southern lowland. Using stratigraphic, geomorphic, and age evidence to correlate earthquakes from site to site, we selected ages that most closely limit the times of late Holocene earthquakes (Table 1; Table S1 in the Supplemental File[1]) and calculated time intervals for each earthquake.

Figure 1 (*on following page*). (A) Kinematic model of the Cascadia forearc (simplified from Wells et al., 1998; Wells and Simpson, 2001). Northward migration of the Oregon Coast Range squeezes western Washington against the North American plate, producing faults and earthquakes in the Puget Lowland. Red lines are faults; black arrows show motions of tectonic blocks. (B) Tectonic setting of the Seattle and Tacoma fault zones and the Saddle Mountain deformation zone in the southern Puget Lowland region (modified from Blakely et al., 2009). The Puget Lowland occupies the area within the orange dashed line. Red and green stipples indicate regions of uplift and sedimentary basins, respectively, as defined by gravity anomalies. Holocene or suspected Holocene faults are shown in black. Faults in the Seattle and Tacoma fault zones and the Saddle Mountain deformation zone are shown in red. Basins and regions of uplift: BB—Bellingham basin; EB—Everett basin; KA—Kingston arch; SB—Seattle basin; SU—Seattle uplift; DB—Dewatto basin; TB—Tacoma basin; OU—Olympia uplift. Faults: BCF—Boulder Creek fault; LRF—Leech River fault; DMF—Devil's Mountain fault; SWIF—southern Whidbey Island fault; RMF—Rattlesnake Mountain fault; SMF—Saddle Mountain faults; CRF—Canyon River fault; FCF—Frigid Creek fault; WRF—White River fault; OF—Olympia fault. (C) Southern Puget Lowland showing the Seattle fault zone, Tacoma fault zone, Saddle Mountain deformation zone, Olympia fault, and related late Holocene fault scarps (base from Finlayson, 2005). Faults (red lines) are inferred from evidence summarized by Brocher et al. (2004), Johnson et al. (2004b), Karel and Liberty (2008), Liberty and Pratt (2008), Witter et al. (2008), Blakely et al. (2009), Clement et al. (2010), and Tabor et al. (2011). Fault scarps (black lines) are as identified on lidar (light detection and ranging) imagery by many investigators (e.g., Harding and Berghoff, 2000; Haugerud and Harding, 2001; Nelson et al., 2002; Haugerud et al., 2003; Sherrod et al., 2004a; Nelson et al., 2008; Witter et al., 2008; Blakely et al., 2009). Colored symbols mark sites with evidence of surface deformation (from Bucknam et al., 1992; Sherrod, 2001; Sherrod et al., 2004a; Tabor et al., 2011; Arcos, 2012): green (inverted triangles)—coseismic subsidence, purple (triangles)—coseismic uplift, blue (circle)—no movement. Faults marked by the Price Lake scarps include the Saddle Mountain East fault (SME) and Saddle Mountain West fault (SMW).

TECTONICS OF THE SEATTLE AND TACOMA FAULTS AND HOLOCENE RUPTURE MODE DIVERSITY

The subsurface geometry of the Seattle fault zone is the subject of debate. Johnson et al. (1994, 1999), Pratt et al. (1997), and ten Brink et al. (2002) interpreted the Seattle fault zone as a complex, south-dipping (~40°) master-ramp thrust (Fig. 3A). Short, south-facing scarps in the central Seattle fault zone, such as along the Toe Jam Hill fault on Bainbridge Island, were interpreted as shallow, north-dipping faults antithetic to the master-ramp fault (Figs. 1C, 2A, and 3A). In a variation of this model (adopted by ten Brink et al., 2006), Brocher et al. (2004) proposed a passive-roof duplex in which the shallow faults root into a gently north-dipping detachment fault above the south-dipping master-ramp fault (Fig. 3B). Liberty and Pratt (2008) proposed that the eastern part of the Seattle fault zone is a thrust fault that extends upward into a fault-propagation fold with a breakthrough forelimb fault (Fig. 3C). The tip of the breakthrough fault forms a blind growth fold and may be the fault exposed in a trench across the Vasa Park scarp (Fig. 1C; Sherrod, 2002).

In the central Seattle fault zone, Kelsey et al. (2008) incorporated aspects of the Brocher et al. (2004) and ten Brink et al. (2006) models, but Kelsey et al. (2008) proposed that the upper part of the fault zone is a doubly vergent, wedge-thrust, fault-bend fold. The north-dipping reverse faults marked by scarps on Bainbridge Island are interpreted as shallow flexure slip, bedding-plane thrust faults that root 4–6 km deep in the active axial surface of the wedge-thrust fold (Figs. 2A and 3D). In this model, the shallow bedding-plane faults may slip during moderate earthquakes independent of slip on the deeper master-ramp thrust.

[1]Supplemental File. PDF file containing two tables and six figures that describe basic data for sites in the paper that are not summarized elsewhere. If you are viewing the PDF of this paper or reading it offline, please visit http://dx.doi.org/10.1130/GES00967.S1 or the full-text article on www.gsapubs.org to view the Supplemental File.

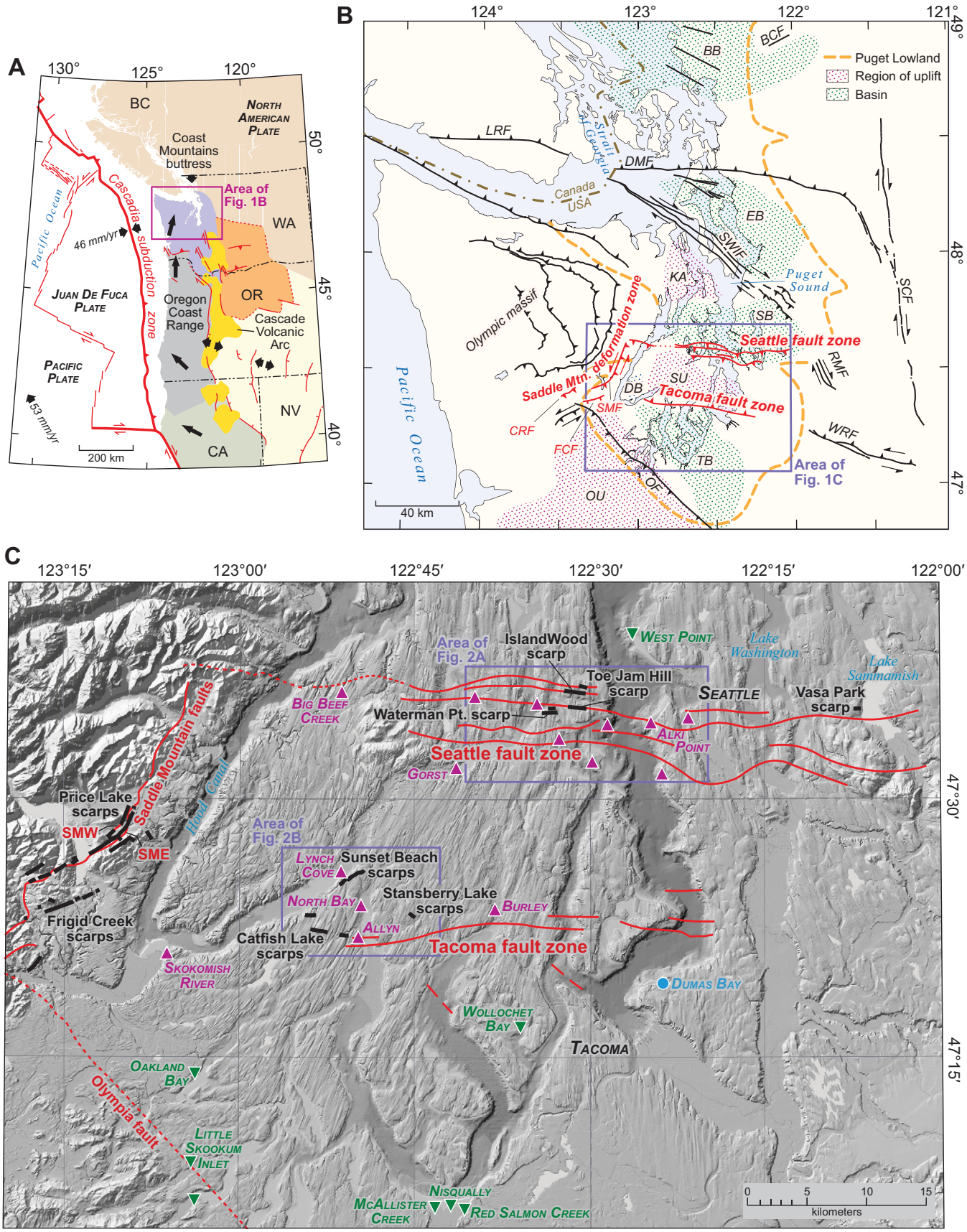
A
130°
125°
120°
50°
45°
40°
BC
North American Plate
Coast Mountains buttress
Area of Fig. 1B
WA
OR
NV
CA
Cascadia subduction zone
Pacific Ocean
46 mm/yr
53 mm/yr
Juan De Fuca Plate
Pacific Plate
Oregon Coast Range
Cascade Volcanic Arc
200 km
B
124°
123°
122°
121°
49°
48°
47°
Puget Lowland
Region of uplift
Basin
BB
BCF
LRF
Strait of Georgia
DMF
Canada
USA
EB
SWIF
KA
Puget Sound
SCF
Olympic massif
SB
Seattle fault zone
deformation zone
Saddle Mtn.
RMF
SU
DB
Tacoma fault zone
SMF
CRF
FCF
WRF
TB
OF
OU
Pacific Ocean
Area of Fig. 1C
40 km
C
123°15′
123°00′
122°45′
122°30′
122°15′
122°00′
47°30′
47°15′
Area of Fig. 2A
IslandWood scarp
West Point
Lake Washington
Lake Sammamish
Toe Jam Hill scarp
Seattle
Vasa Park scarp
Big Beef Creek
Waterman Pt. scarp
Alki Point
Seattle fault zone
Gorst
Saddle Mountain faults
Hood Canal
Price Lake scarps
SMW
SME
Area of Fig. 2B
Lynch Cove
Sunset Beach scarps
North Bay
Stansberry Lake scarps
Burley
Allyn
Frigid Creek scarps
Catfish Lake scarps
Tacoma fault zone
Skokomish River
Dumas Bay
Wollochet Bay
Tacoma
Oakland Bay
Olympia fault
Little Skookum Inlet
McAllister Creek
Nisqually
Red Salmon Creek
0
5
10
15
kilometers

Figure 1.

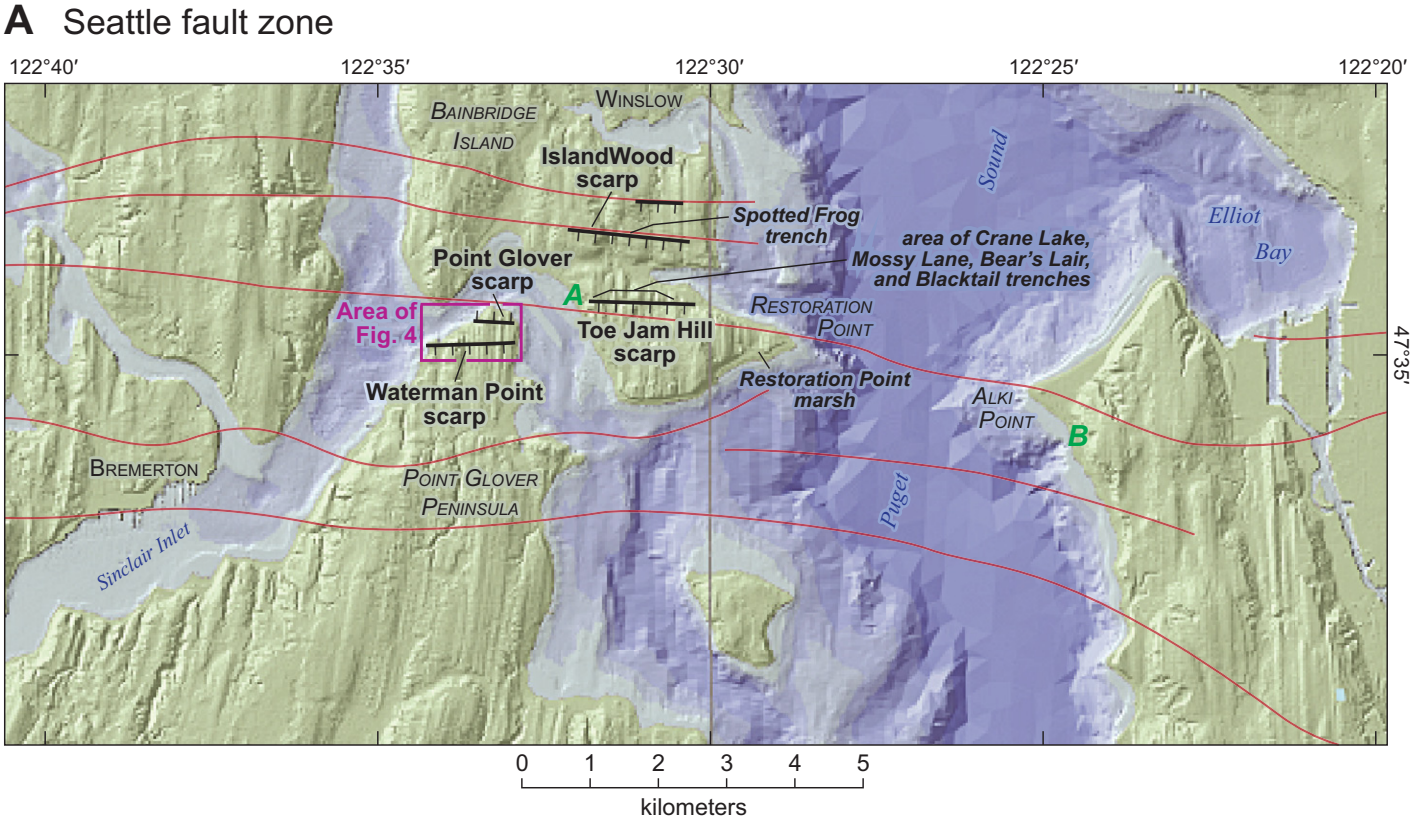

Figure 2. Maps of fault scarps and sites with evidence of surface deformation in (A) the central Seattle fault zone and (B) the central Tacoma fault zone (located in Fig. 1C; base from Finlayson, 2005). Hachures on fault scarps (black lines) point down the scarp. Projected surface traces of major faults at depth (light red lines) are from Figure 1C. Green letter A locates the intersection of the Toe Jam Hill fault scarp with marine terraces on the west coast of Bainbridge Island. Green letter B locates a strand of the Seattle fault south of Alki Point. The pronounced north-to-northeast trend of landforms was produced during glaciation of the Puget Lowland. Much higher resolution lidar (light detection and ranging) imagery of scarps in A is shown with trench site locations in Nelson et al. (2002, fig. 2 therein, http://pubs.usgs.gov/of/2002/ofr-02-0060/; 2003b, Fig. 2 therein, http://pubs.usgs.gov/mf/2003/mf-2423/) and Kelsey et al. (2008, fig. 1B therein), and in B in Sherrod et al. (2004a, fig. 3 therein) and Nelson et al. (2008, figs. 3, 4, 10, 11, and 12 therein, http://pubs.er.usgs.gov/usgspubs/sim/sim3060).

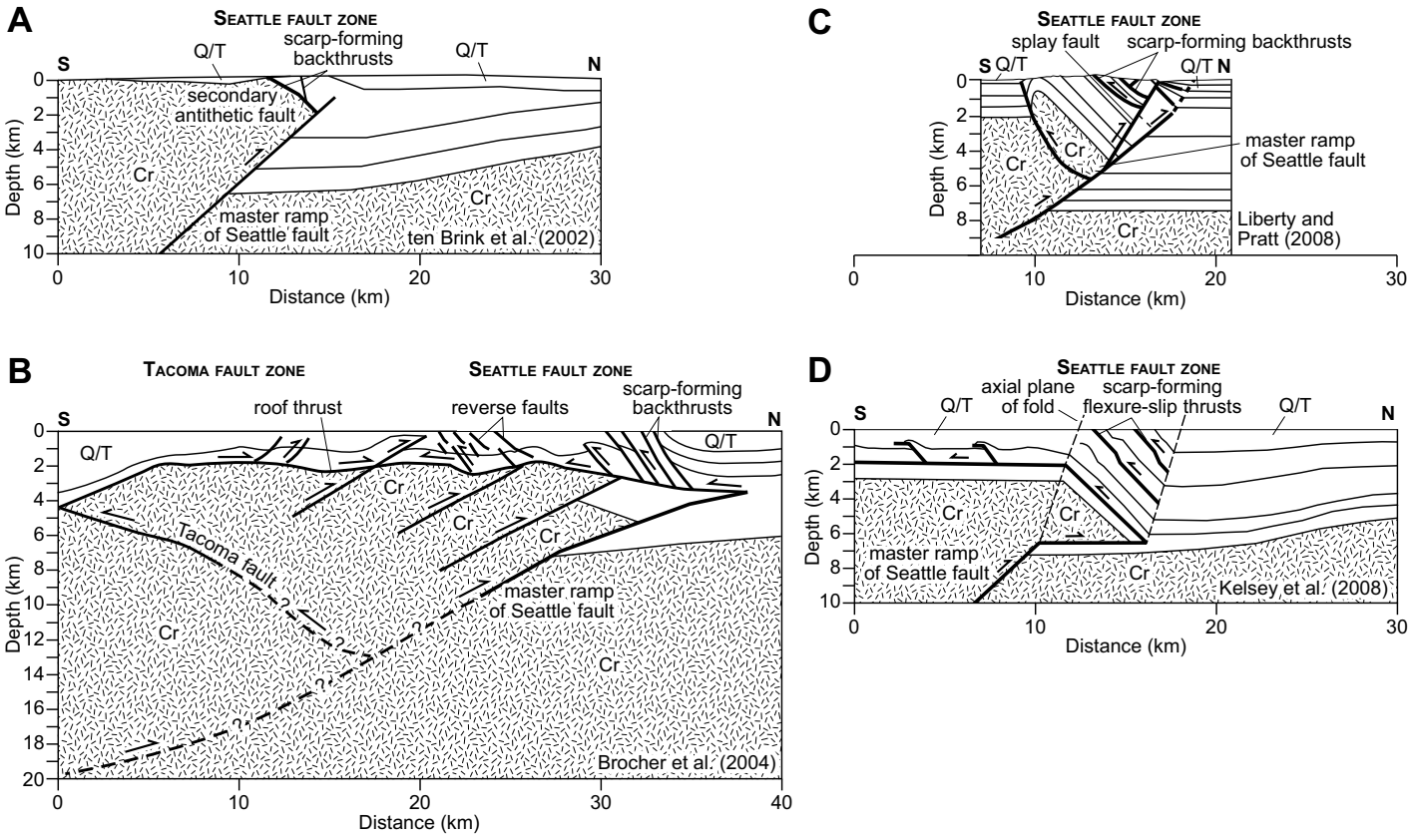

Figure 3. Cross sections illustrating structural models of the Seattle fault zone and its relation to the Tacoma fault zone (from labeled studies); A, B, and C are modified from figures in Kelsey et al. (2008). Models A, B, and D, for the central part of the Seattle fault zone, are partly based on interpretations of north-south seismic reflection profiles east of Bainbridge Island (Fig. 2A), whereas model C is for the eastern part of the fault zone near Lake Washington (Liberty and Pratt, 2008). The main thrust of the Tacoma fault is shown only in model B. Cr—Crescent Formation; Q—Quaternary; T—Tertiary. (A) Scarp-forming backthrusts (marked by scarps such as the IslandWood scarp, the Toe Jam Hill scarp, and the Waterman Point scarp; see Fig. 2A) are antithetic to the blind master-ramp thrust of the Seattle fault. (B) A passive roof thrust soles into the blind master-ramp thrust of the Seattle fault, and scarp-forming backthrusts sole into the roof thrust. (C) Scarp-forming backthrusts are antithetic to steeply dipping splay faults that sole in the blind master-ramp thrust of the Seattle fault. (D) Scarp-forming, flexure-slip, bedding-plane thrust faults root in the active axial surface of a wedge-thrust fold above the blind master-ramp thrust of the Seattle fault. In all models, slip on the scarp-forming thrusts could occur during slip on the master-ramp thrust during large or very large earthquakes. For D, Kelsey et al. (2008) argued that slip on the scarp-forming thrusts also occurs during shallow (<5 km depth) moderate-magnitude earthquakes independent of slip on the master-ramp thrust. Although the Tacoma fault may sole into the master-ramp thrust of the Seattle fault as shown in B, slip on the Tacoma fault does not necessarily occur during slip on the Seattle fault.

The Tacoma fault zone consists of a series of faults and folds with a north-dipping reverse fault on its western end, a growth fold above a deeper fault beneath Case Inlet, and a fault that intersects a northwest-trending monocline on its eastern end (Figs. 1C, 2B, and 3B; Pratt et al., 1997; Brocher et al., 2001, 2004; Johnson et al., 2004b). Shallow seismic reflection work has confirmed the growth fold and other folds to the west, and identified small faults near the northwest-trending monocline that indicate its postglacial growth. Clement et al. (2010) interpreted the reflection data to suggest Holocene folding and faulting along the Olympia fault (or fold) on the south edge of the Tacoma basin. If north-dipping reverse faults of the Tacoma fault zone sole into a south-dipping master Seattle thrust, they do so at a depth of at least 10 km (Fig. 3B; Brocher et al., 2001, 2004; Johnson et al., 2004b; Clement et al., 2010).

The different structural models affect interpretations of the magnitude of the earthquakes recorded by fault scarps and deformed shorelines in the Seattle and Tacoma fault zones. All of the models are consistent with the largest earthquakes being produced during ruptures tens of kilometers long on the master-ramp thrust of the Seattle fault zone and/or on faults of the Tacoma fault zone that extend deeper than 8–10 km. Kelsey et al. (2008) termed these "regional earthquakes," based on shorelines uplifted >3 m over an area 5–6 km wide and tens of kilometers long on the hanging wall of the Seattle fault zone during the Restoration Point earthquake. We refer to these largest upper plate earthquakes as "very large," and follow previous studies in inferring that they were M 7–7.5 (e.g., Bucknam et al., 1992; Sherrod, 2001; Blakely et al., 2009).

As interpreted in Kelsey et al. (2008), earthquakes recorded by short scarps or uplifted terraces extending <1–2 km from faults may have rupture areas limited to the upper 4–6 km of a fault-bend-fold wedge over distances of 8–10 km (Fig. 3D). These events were considered "local earthquakes" by Kelsey et al. (2008) with inferred "moderate" magnitudes of 5.5–6.0. If instead, the ruptures with limited

TABLE 1. LATE HOLOCENE RADIOCARBON AGES THAT CLOSELY LIMIT THE TIMES OF SURFACE DEFORMATION IN THE SEATTLE AND TACOMA FAULT ZONES AND SADDLE MOUNTAIN DEFORMATION ZONE

Lab-reported age (^{14}C yr B.P. at 1σ)*	Calibrated age (cal yr B.P. at 2σ)†	Calibrated age (cal yr A.D. at 2σ)†	Inferred age context§	Description of dated material**
Seattle fault zone				
Bainbridge Island				
Winslow marsh—Eagle Harbor (Bucknam et al., 1992)				
1081 ± 66	**1170–800**	**780–1150**	**max D**	wood in peat
Spotted Frog trench—IslandWood scarp (this paper)				
1290 ± 40	1290–1160	660–790	max D	charcoal fragments
Bear's Lair trench—Toe Jam Hill scarp (Nelson et al., 2002, 2003a)				
1160 ± 50	**1230–960**	**720–990**	**close max D**	*Thuja plicata* leaf attached to block of mud
Saddle trench—To Jam Hill scarp (Nelson et al., 2002, 2003a)				
3020 ± 50	3360–3060	–1410– –1130	max B	charcoal fragments
Mossy Lane trench—Toe Jam Hill scarp (Nelson et al., 2002, 2003a)				
1230 ± 30	**1270–1060**	**690–880**	**close min C** and max D	charred bark
1300 ± 21	**1290–117**	**660–770**	**close min C** and max D	outermost 7–10 rings of charcoal log
1360 ± 40	**1350–1170**	**600–770**	**close max C**	three 3-mm-long charcoal fragments
1410 ± 40	**1390–1260**	**570–670**	**close max C**	5-mm-long charcoal fragment
Blacktail trench—Toe Jam Hill scarp (Nelson et al., 2002, 2003a)				
980 ± 80	**1060–720**	**890–1220**	**min D?**	pieces of charcoal
1340 ± 45	1330–1170	6220–770	max D?	charcoal fragment
1320 ± 40	1330–1170	650–770	max C or D	two fragments of slightly abraded wood
Crane Lake trench—Toe Jam Hill trench (Nelson et al., 2002, 2003a)				
1060 ± 30	**1060–920**	**900–1020**	**close max D**	clean charcoal sticks from forest floor
1240 ± 50	1290–1050	670–890	max D	charcoal fragment
1290 ± 30	1290–1170	660–770	max D	charcoal fragment
1470 ± 40	1490–1290	470–650	min C	three charcoal fragments
1520 ± 40	1520–1310	430–620	max C	charcoal fragments, largest with twig morphology
1810 ± 60	1880–1560	70–380	max C	pieces of clean charcoal
2010 ± 30	**2050–1880**	**–90–70**	**min B**	decayed charcoal fragment
2440 ± 30	**2720–2350**	**–750– –410**	**max B**	charcoal fragment
2550 ± 30	**2750–2498**	**–800– –550**	**max B**	clean charcoal fragment
Point Glover area				
Snowberry trench—Waterman Point scarp (Nelson et al., 2003b)				
1117 ± 26	**1070–960**	**880–990**	**close max D**	split 15 × 15 × 10 mm fragment from bed of charcoal
1000 ± 40	**980–790**	**970–1150**	**max E**	10 × 5 × 4 mm fragment from bed of charcoal
Madrone Ridge trench—Waterman Point scarp (Nelson et al., 2003b)				
1540 ± 35	1520–13560	430–590	max E	15 × 4 × 4 mm charcoal fragment
1601 ± 25	1540–1410	410–540	max E	split 13 × 6 × 4 mm charcoal fragment into halves
1300 ± 30	1290–1180	660–770	max D	five 5 × 3 × 2 mm dense charcoal fragment
1290 ± 35	1290–1140	650–800	max D	one 5 × 2 × 1 and two 8 × 4 × 20mm charcoal fragments
Nettle Grove trench—Waterman Point scarp (this paper)				
1181 ± 26	**1180–1010**	**770–940**	**close max D**	split 20 × 10 × 5 mm charcoal fragment in halves
Madrone East core transect—Waterman Point scarp (this paper)				
735 ± 35	730–570	1220–1380	min D	5 × 8 mm hard woody seed, *Prunus* type
1220 ± 40	1270–1060	680–890	close max D	7 × 4 mm hard woody seed, *Prunus* type
Wataugua Beach West core site—Waterman Point scarp (this paper)				
925 ± 40	**930–740**	**1020–1210**	**close max E and close min D**	14-mm-long *Pseudotsuga menziesii* twig
1025 ± 40	**1050–800**	**900–1150**	**max E**	21 *P. Menziesii* leaves + *Tsuga heterophylla* bract
1005 ± 40	**1050–790**	**900–1150**	**close min D and max E**	6 × 12mm fresh herb bract or bud
1150 ± 30	**1170–980**	**780–970**	**close max D**	12-mm-long twig with bark and petioles
Gorst wetland—Sinclair Inlet (Arcos, 2012)				
700 ± 40	**710–560**	**1240–1390**	**min D**	*Tsuga heterophylla* cone 2 cm above sand
1100 ± 25	**1060–960**	**890–990**	**close max D**	deciduous leaf in lower 5 cm of debris flow deposit
1190 ± 30	**1230–1010**	**720–940**	**max D**	deciduous leaf in lower 5 cm of debris flow deposit
1240 ± 30	**1260–1070**	**680–870**	**max D**	deciduous leaf in lower 5 cm of debris flow deposit
East of Puget Sound				
West Point—excavation of tsunami-deposited sand (Atwater, 1999; Sherrod, 2001)				
1100 ± 15	1060–960	890–990	close max D	outer 15 rings of tsunami-deposited log
1108 ± 16	1060–960	890–990	close min D	*Scirpus*-type stems in tsunami-deposited sand
wiggle match of 5 ages	**1050–1020**	**900–930**	**round-number age interval D**	log in tsunami-deposited sand

(*continued*)

TABLE 1. LATE HOLOCENE RADIOCARBON AGES THAT CLOSELY LIMIT THE TIMES OF SURFACE DEFORMATION IN THE SEATTLE AND TACOMA FAULT ZONES AND SADDLE MOUNTAIN DEFORMATION ZONE (*continued*)

Lab-reported age (^{14}C yr B.P. at 1σ)*	Calibrated age (cal yr B.P. at 2σ)†	Calibrated age (cal yr A.D. at 2σ)†	Inferred age context§	Description of dated material**
Tacoma fault zone				
North of Tacoma fault				
Lynch Cove marsh—Hood Canal (Bucknam et al., 1992; Sherrod, 2001)				
1170 ± 90	**1270–930**	**680–1020**	**close min D**	peat
1132 ± 17	**1170–960**	**780–990**	**close min D**	leaf bases of *Triglochin maritima*
1159 ± 14	**117–980**	**780–960**	**close max D**	trunk of small tree embedded in sand
1050 ± 70	**1170–960**	**780–1160**	**close max D**	woody root in growth position
Snake trench—Sunset Beach scarps (Nelson et al., 2008)				
1280 ± 45	1290–1080	660–870	max D	5 × 5 × 4 mm fragile charcoal fragment
Bee's Nest trench—Sunset Beach scarps (Nelson et al., 2008)				
1280 ± 40	1290–1080	660–860	max D	6 × 2 × 1 mm charcoal fragment
Burley marsh (Bucknam et al., 1992; Sherrod et al., 2004a, 2004b)				
1130 ± 50	**1180–950**	**780–1010**	**close min D**	leaf base of *Triglochin maritima* from basal peat
Micah trench—Stansberry Lake scarp (Nelson et al., 2008)				
1240 ± 85	1300–980	650–970		8 × 3 × 2 mm partially burned fragment, outer 10 mm root
1080 ± 25	1050–930	890–1020		15 × 15 × 2 mm fragment from outer 10 mm of root
1110 ± 30	1070–940	880–1010		8 × 6 × 2 mm platy charcoal fragment
1100 ± 19	**1060–960**	**890–990**	**close min D**	3-age mean from burned root in scarp colluvium
1580 ± 30	1530–1400	410–550	max D	5 × 4 × 1 mm platy charcoal fragment
Catfish Lake and Mill Pond—Catfish Lake scarps (Logan and Walsh, 2007)				
1140 ± 50	**1180–940**	**770–1010**	**close max D**	wood from stump in Catfish Lake
1290 ± 60	1300–1070	650–880	max D	wood from stump in Catfish Lake
1240 ± 60	1290–1010	660–940	max D	wood from stump in Mill Pond
1260 ± 60	1290–1060	660–890	max D	wood from stump in Mill Pond
Allyn marsh—Catfish Lake scarps (Sherrod et al., 2004a, 2004b)				
1040 ± 40	**1060–830**	**890–1120**	**close min D**	seeds
South of Tacoma fault				
Wollochet Bay marsh (Sherrod et al., 2004a, 2004b)				
970 ± 50	970–760	980–1180	close max D?	outermost rings *Pseudotsuga menziesii* stump
Nisqually marsh (Sherrod, 2001)				
1030 ± 70	**1170–780**	**780–1170**	**close min D**	leaf bases of *Triglochin maritima*
Nisqually—McAllister Creek marsh (Sherrod, 2001)				
1140 ± 80	**1260–930**	**690–1020**	**min D**	leaf bases of *Triglochin maritima*
Nisqually—Red Salmon Creek marsh (Sherrod, 2001)				
1010 ± 50	**1050–790**	**900–1160**	**close max D**	outermost rings *Pseudotsuga menziesii* stump
1200 ± 14	1180–1060	770–890	max D	*Pseudotsuga menziesii* stump
wiggle match age	**1090–1010**	**860–940**	**close max D**	*Pseudotsuga menziesii* stumps
Little Skookum Inlet marsh (Sherrod, 2001)				
1090 ± 60	**1170–920**	**780–1030**	**close max D**	outer 15–25 rings of *Pseudotsuga menziesii* stump
1222 ± 15	1260–1017	690–880	max D	rings (offset 83 yr) in *Pseudotsuga menziesii* stump

(*continued*)

areas of surface deformation sole in a master thrust when it slips during earthquakes (ten Brink et al., 2002; Brocher et al., 2004; Liberty and Pratt, 2008; Pratt and Troost, 2009), rupture areas would be at least an order of magnitude larger, likely generating "large" earthquakes of ~M 6.5–7.0 (Figs. 3A, 3C). If large, these earthquakes apparently produced less than meters of surface deformation over areas less than kilometers wide and tens of kilometers long.

Farther west, Witter et al. (2008) and Blakely et al. (2009) argued that postglacial movement on faults of the Saddle Mountain deformation zone help accommodate northward-directed slip on the deep thrusts of the Seattle fault zone where it may impinge on the southeast flank of the Olympic Mountains (Fig. 1C; Polenz et al., 2011). Blakely et al. (2009) concluded that an earthquake on the Saddle Mountain fault ca. 1000–1300 cal yr B.P. was M 6.5–7, what we term a "large earthquake."

Typical 50–200-yr analytical uncertainties and additional stratigraphic and sample context uncertainties in ^{14}C dating (Sherrod, 2001; Nelson et al., 2003a; Kemp et al., 2013) preclude distinguishing individual earthquakes on the Seattle fault zone, the Tacoma fault zone, and the Saddle Mountain deformation zone that occurred ~1000 cal yr B.P. Because our paleoseismic methods cannot distinguish between a series of large earthquakes or one very large earthquake ~1000 cal yr B.P. on these faults, we refer to surface-deforming earthquakes within ~100–200 yr of 1000 cal yr B.P. as within the "millennial earthquake series." We term the largest earthquake of the millennial series, first identified from extensive uplifted shorelines on Bainbridge Island (Fig. 2A; Bucknam et al., 1992; Sherrod et al., 2000), the Restoration Point earthquake. Based on less distinct and spatially much more limited stratigraphic and geomorphic earthquake evidence, other, probably smaller, surface-deforming earthquakes in the Seattle fault zone and possibly the Tacoma fault zone occurred before (Nelson et al., 2003a; Kelsey et al., 2008) and after (Sherrod, 2001; Nelson et al., 2003c; Karlin et al., 2004) the Restoration Point earthquake. Although ^{14}C ages that limit the times of surface faulting or folding help us interpret the evidence of other earthquakes, in most cases the ages are merely consistent with site-to-site correlations of earthquakes based on stratigraphic and geomorphic evidence (Sherrod, 2001; Nelson et al., 2003a;

TABLE 1. LATE HOLOCENE RADIOCARBON AGES THAT CLOSELY LIMIT THE TIMES OF SURFACE DEFORMATION IN THE SEATTLE AND TACOMA FAULT ZONES AND SADDLE MOUNTAIN DEFORMATION ZONE (*continued*)

Lab-reported age (^{14}C yr B.P. at 1σ)*	Calibrated age (cal yr B.P. at 2σ)†	Calibrated age (cal yr A.D. at 2σ)†	Inferred age context§	Description of dated material**
Saddle Mountain deformation zone				
Price Lake—Saddle Mountain East faults (Wilson et al., 1979; Jacoby et al., 1992; Hughes, 2005; Polenz et al., 2011)††				
1155 ± 85	**1270–930**	**680–1020**	**close max Dsmw**	submerged stump in pond
1315 ± 80	1370–1060	580–890	max Dsme	stump submerged 3.4 m in Price Lake
—	1290–1080		max Dsme	conifer cones and needles; range of 2 concordant ages
—	1270–1050		max Dsme	*Tsuga heterophylla* cone
1150 ± 40	**1170–970**	**660–870**	**close max Dsmw**	*Tsuga heterophylla* needles
1210 ± 35	**1260–1060**	**690–890**	**close max Dsmw**	*Thuja plicata* cone
1230 ± 40	1270–1060	680–890	max Dsme	leaves of wetland plants
1240 ± 30	1260–1070	680–870	max Dsme	wetland seed mixture
1250 ± 30	1270–1080	680–870	max Dsme	*Thuja plicata* cone
1270 ± 40	1290–1080	660–870	max Dsme	*Tsuga heterophylla* needles
Price Lake—Saddle Mountain West faults (Hughes, 2005; Polenz et al., 2011)				
1210 ± 40	**1260–980**	**690–940**	**close max Dsmw**	*Tsuga heterophylla* needles
1220 ± 40	1270–1060	680–890	max Dsmw	submerged *Pseudotsuga menziesii* stump
1250 ± 40	1280–1080	670–870	max Dsmw	submerged *Pseudotsuga menziesii* stump
Cargill Creek trench—Saddle Mountain West fault (Witter et al., 2008)				
1120 ± 35	1170–940	780–1010	**min Dsmw** or max Dsmw?	charcoal in colluvium

*Radiocarbon age reported by laboratory. Laboratory sample numbers and more complete data in Table S1 (see text footnote 1). Ages in bold most closely constrain the times of earthquakes; calibrated age column data were used in the OxCal analysis (see text Figs. 5 and 6) to calculate time-interval probability distributions for each earthquake. Other ages constrain earthquake timing less closely, but support the calculated time intervals. Two ages conflict with the calculated intervals (see text).

†Ages in solar years calculated using OxCal (version 4.1; Bronk Ramsey, 1995, 2009; probability method) with the INTCAL09 data set of Reimer et al. (2009) rounded to the nearest decade. Calibrated ages show time intervals of >95% probability distribution at 2σ. Ages shown in figures (ka; see text) are weighted averages of probability distribution functions (Telford et al., 2004) rounded to nearest 100 yr.

§Interpretation of the stratigraphic context of dated samples that most closely limit the times of surface faulting and folding. Maximum (max) limiting ages are on samples containing carbon judged to be older than the earthquake, minimum (min) limiting ages are on samples judged younger than the earthquake, and close ages are those on samples judged to contain carbon produced within a few decades of the earthquake. Context, sample type, and sample quality were used to infer whether age is a maximum age, minimum age, or close maximum age. Earthquake labels are those of Nelson et al. (2003a; B, C, and D) with the addition of a younger earthquake (E) and a separate earthquake or earthquakes (Dsme and Dsmw) in the Saddle Mountain deformation zone (sme—Saddle Mountain East; smw—Saddle Mountain West).

**Unless indicated otherwise, ages are on unabraded fragments of wood charcoal. In each sample, the largest, most angular, least decayed fragments of charcoal, wood, and/or above-ground plant parts were selected to minimize the chance of analyzing carbon much older than the host sediment. In most samples, fragments with root-like morphology were avoided to minimize the chance of analyzing roots much younger than the host sediment. Except for a few of the most delicate fragments, rootlets and sediment adhering to fragments were removed with brushes or dental tools in distilled water at 12–50×.

††We list only the six ages that Polenz et al. (2011, Appendix A therein) described as the closest maximum limiting ages on the time of forest and soil submergence in Price Lake due to faulting.

Kelsey et al., 2008). We return to the topic of rupture extent during the millennial earthquake series in the Discussion.

LATE HOLOCENE DEFORMATION IN THE SEATTLE FAULT ZONE

Most evidence of surface deformation during earthquakes of the past few thousand years in the Seattle fault zone have come from studies of fault scarps and deformed shorelines on Bainbridge Island and the Point Glover peninsula to the south (Figs. 1C and 2A; Table 1; Table S1 in the Supplemental File [see footnote 1]). Other sites with evidence of surface deformation include Alki Point near Seattle, Vasa Park in the eastern part of the fault zone (Sherrod, 2002), and sites along faults of the Saddle Mountain deformation zone. In this section, we summarize earlier investigations in the central Seattle fault zone, describe new evidence for surface-rupturing earthquakes along scarps, and explain how deformed shorelines are related to earthquakes.

Methods used to investigate surface deformation were discussed by Nelson et al. (2003a, 2003b), Sherrod et al. (2004a, 2008), Witter et al. (2008), and Blakely et al. (2009). All basic data for scarp sites, such as complete trench logs, core descriptions, scarp topographic profiles, detailed descriptions and interpretations of stratigraphic units, notes explaining how fault slip was measured, and tables of lithologic, radiocarbon, structural, soil profile, and paleoecologic data can be found in Nelson et al. (2002, 2003b, 2008), Sherrod et al. (2004b), Witter et al. (2008), or in the Supplemental File (see footnote 1). Shoreline site methods were described in Sherrod et al. (2000), Sherrod (2001), and Kelsey et al. (2008). Our analysis and interpretation of key ^{14}C ages from sites in the central Seattle fault zone follow the discussion of surface deformation data.

Previous Investigations of Surface Deformation

Deformed Shorelines and Earthquake Dating

Beginning with the shoreline studies of Bucknam et al. (1992), investigators have attributed most uplifted shorelines in the central Seattle fault zone to uplift of the fault hanging wall during the Restoration Point earthquake. These include uplifted marine platforms located at Restoration Point, 5 km to the east at Alki Point, and along the shores of southern Bainbridge Island and the Point Glover peninsula (Figs. 1C, 2A, and 4; Table 1; Table S1 in the Supplemental File [see footnote 1]; e.g., Atwater and Moore, 1992; Sherrod et al., 2000; Harding et al., 2002; Ota et al., 2006; Kelsey et al., 2008). Conversely, the marsh at Winslow, 5 km north of Restoration Point on the footwall of the fault (Fig. 2A), probably subsided during the earthquake, as did West Point ~4 km north of the uplifted platform at Alki Point (Fig. 1C; Atwater and Moore, 1992; Bucknam et al., 1992; Ekblaw and Leopold, 1993). Maximum and minimum limiting ^{14}C ages for uplift and subsidence in these studies placed the earthquake between 550 and 1750 cal yr B.P. (Table 1; Table S1 in the Supplemental File [see footnote 1]; Bucknam et al., 1992). Shoreline uplift and a tsunami, caused by slip on faults of the Seattle zone, were dated at Gorst to 1260–560 cal yr B.P. (Fig. 1C; Arcos, 2012).

More precise ages for the Restoration Point earthquake came from matching ^{14}C ages on different-aged groups of outer ring wood from trees that died about the time of the earthquake with fluctuations in the radiocarbon calibration curve (e.g., Kemp et al., 2013). In an excavation

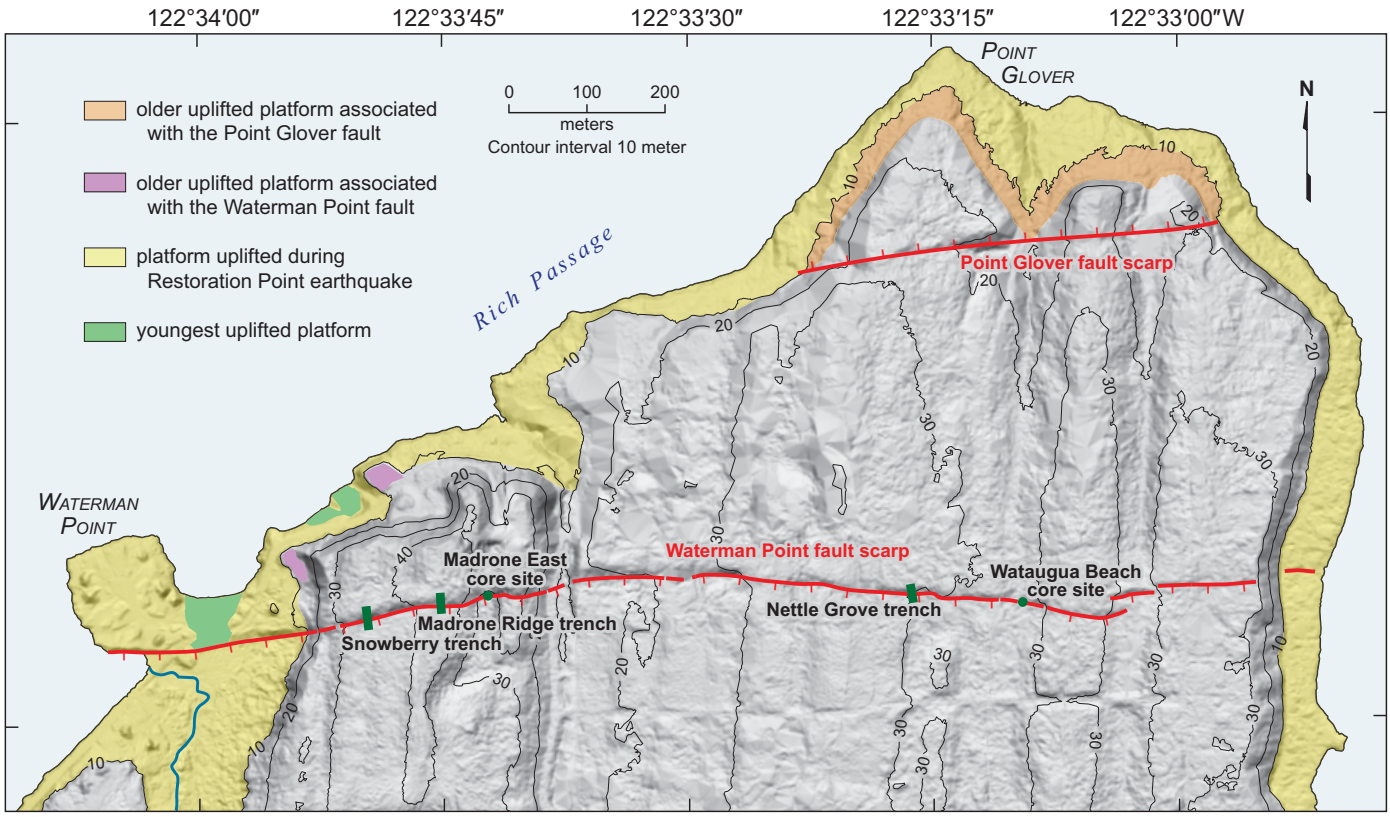

Figure 4. Lidar (light detection and ranging) imagery and topographic map (located in Fig. 2A) of the northern part of the Point Glover peninsula showing the scarps of the Waterman Point and Point Glover faults, uplifted shoreline platforms, and trench and coring sites. The linear feature 200 m south of the Waterman Point scarp and parallel to it is a road. Figure 2 of Nelson et al. (2003b, http://pubs.usgs.gov/mf/2003/mf-2423/) shows the location of trench and core sites on a high-resolution lidar image of the fault scarps with 1 m contours. Hachures on fault scarps point down the scarp. As described by Kelsey et al. (2008), the wide, continuous platform extending around both sides of the peninsula was uplifted during the Restoration Point earthquake. An older platform uplifted during slip on the Point Glover fault is just north of that fault. We also mapped two small remnants of an older platform uplifted during slip on the Waterman Point fault <200 m north of the fault, but whether the remnants are older or younger than the older platform north of the Point Glover fault is uncertain. The two remnants of a youngest platform 4 m below the continuous platform and <380 m east of Waterman Point may have been uplifted during the younger of two earthquakes on the Waterman Point fault. The pronounced northward trend of landforms was produced during glaciation of the Puget Lowland.

at West Point, Atwater and Moore (1992) identified deposits of the tsunami produced by sudden upper plate uplift during the earthquake. *Scirpus* sp. stems engulfed by sand exposed in the excavation were flattened by a log carried by the tsunami. By wiggle matching three ages on groups of rings from the log, Atwater (1999) narrowed the time of the earthquake to 1050–1020 cal yr B.P. (Table 1; Fig. 5). Close agreement among ages on *Scirpus* stems and log ages, and the good preservation of bark encircling the log, showed that log death did not predate the tsunami by more than a few years. Matching tree-ring patterns among the West Point log and the stumps of trees carried into Lake Washington (Fig. 1C) by shaking-induced landslides showed that the log and stumps probably died in the same season of the same year (Jacoby et al., 1992; Karlin and Abella, 1992). South of the Tacoma fault zone at Red Salmon Creek, Sherrod (2001) also used wiggle-matched ages from the rings of a *Pseudotsuga menziesii* stump, inferred to have been killed by coseismic subsidence, to date subsidence during a large earthquake to 1090–1010 cal yr B.P. (Table 1; Figs. 1C and 5).

Kelsey et al. (2008) inferred, as had previous researchers (e.g., Bucknam et al., 1992; Sherrod et al., 2000; Ota et al., 2006), that the widely distributed, largely continuous, uplifted marine platform in the Seattle fault zone was raised during the Restoration Point earthquake. They interpreted older, higher platforms that merge with the younger continuous platform within hundreds of meters of fault scarps as markers of fault slip during older earthquakes (Fig. 4). Because of the limited extent of the older terraces and their identification at only a few sites, Kelsey et al. (2008) inferred the older terraces to record uplift during moderate magnitude earthquakes on fault-bend-fold faults having lengths of <10 km. At three principal sites, i.e., where the scarp of the Toe Jam Hill fault intersects the west coast of Bainbridge Island (A in Fig. 2A), at the tip of the Point Glover peninsula (Fig. 4), and where a strand of the Seattle fault intersects Puget Sound south of Alki Point (B in Fig. 2A), the uplifted lower shoreline platforms, correlated with the similar platform at Restoration Point, are 2–9 m above Puget Sound. The older platforms on the hanging walls of the faults are ~3 m (west Bainbridge), ~4 m (Point Glover), and ~5 m (Alki Point) higher than the wider, more continuous, lower platforms (terrace maps and profiles in Kelsey et al., 2008, figs. 4–6 therein). If gradual subsidence followed coseismic uplift at many of these sites, as illustrated by stratigraphy and fossils for the Restoration

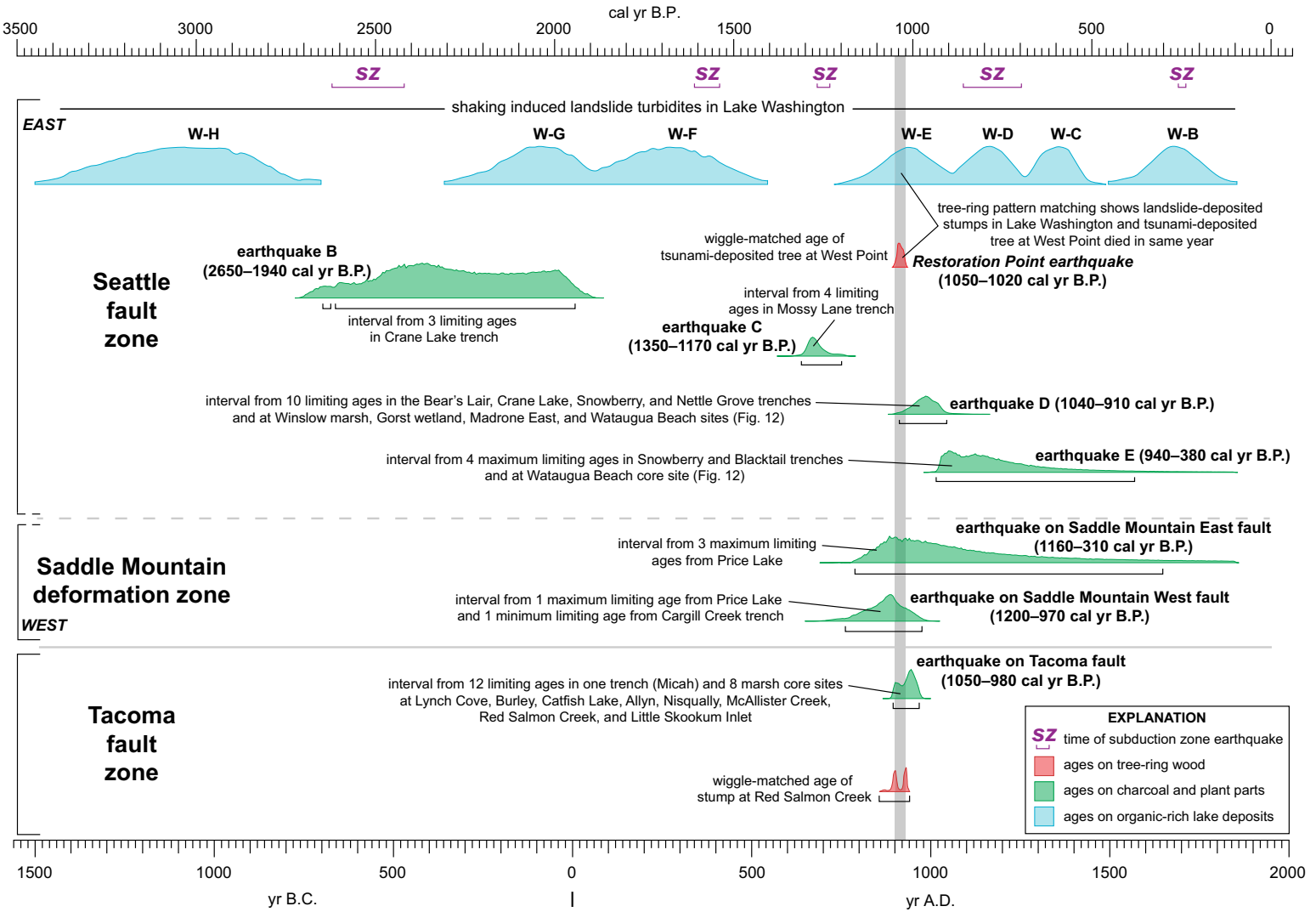

Figure 5. OxCal modeled probability distributions for the times of late Holocene surface-deforming earthquakes in the Seattle fault zone, Tacoma fault zone, and Saddle Mountain deformation zone. Distributions (2σ) for earthquakes B and C (Nelson et al., 2003a), and earthquakes of the millennial earthquake series (Restoration Point earthquake, earthquakes D and E in the Seattle fault zone, and earthquakes in the Tacoma fault zone and Saddle Mountain deformation zone) were calculated using ages listed in bold in Table 1 (see Fig. 12). Distributions for Lake Washington landslide turbidite deposits (from Karlin et al., 2004; blue) were calculated from ages on organic fractions of lake sediment. The bars below purple SZ labels show the time ranges of subduction zone earthquakes with evidence of coastal subsidence from Atwater et al. (2004) and Nelson et al. (2006). The width of turbidite distributions makes it uncertain which turbidites may have been deposited as a result of strong shaking during Cascadia subduction zone earthquakes. Wiggle-matched age distribution for the tsunami-deposited log at West Point is from Atwater (1999) and Sherrod (2001). Vertical gray bar shows time interval for the Restoration Point earthquake (1050–1020 cal yr B.P.) based on the West Point distribution. We calculated separate time intervals for earthquakes on the Saddle Mountain (Mt.) East and Saddle Mountain West faults (see Table 1; ages of Hughes, 2005, as listed in Polenz et al., 2011). Distribution for the wiggle-matched age at Red Salmon Creek is from Sherrod (2001). Because four of the five distributions for earthquakes of the millennial earthquake series overlap with the distribution for the Restoration Point earthquake, we cannot preclude that any of the ruptures of these earthquakes did not occur during the Restoration Point earthquake.

Point earthquake at Gorst (Fig. 1C), the present heights of many shorelines may be minimum values for coseismic uplift (Arcos, 2012).

Toe Jam Hill Fault Scarp

The scarp of the Toe Jam Hill fault extends east-west 1.5 km across the southern part of Bainbridge Island in the Seattle fault zone (Figs. 1C and 2A). A synthesis of stratigraphy and ^{14}C ages from 5 trenches across the 1–6-m-high scarp yielded a history of 3, or possibly 4, surface-rupturing earthquakes between 2.5 and 1.0 ka (Nelson et al., 2003a; site maps and complete data in Nelson et al., 2002).

Charcoal ^{14}C ages from faulted and folded forest soil A horizons date two of the earthquakes, labeled B and C, to ca. 2.5 to 1.9 ka, primarily in the Crane Lake and Mossy Lane trenches. From correlations of earthquakes among trenches (Nelson et al., 2003a), only 3 ages limit the time of the second oldest earthquake (earthquake B), placing it in a 700-yr interval (Fig. 5; Table 1). Charcoal ages from A horizons that most closely constrain the time of earthquake C indicate an age of ca. 1.7–1.2 ka from the Crane Lake trench and ca. 1.3–1.2 ka from the Mossy Lane trench. If earthquakes C and D were correctly correlated by Nelson et al. (2003a) between the two trenches, the youngest maximum age and oldest minimum age from the Mossy Lane trench date earthquake C to 1350–1170 cal yr B.P. (Fig. 5; Table 1). The three other trenches lack firm evidence of earthquake C. The earliest possible earthquake (A), dated between 2.5 ka and 1.9 ka in the Crane Lake trench, may record a toppled tree rather than an earthquake.

Nelson et al. (2003a) correlated the youngest surface-deforming earthquake (earthquake D) in the five trenches with the Restoration Point earthquake. Evidence for the correlations included the youngest detrital ^{14}C ages in the 1.3–1.0 ka range and the relative amount of fault slip or uplift, which was inferred from stratigraphic relations to be largest for the youngest earthquake in 3 of the 5 trenches. Eight ^{14}C ages from the 5 trenches were interpreted as maximum ages for the time of earthquake D (Table 1). The two highest quality samples from the trenches, inferred to predate the earthquake by decades, gave maximum ages for earthquake D of 1230–960 cal yr B.P. (cedar leaf at base of fissure in Bear's Lair trench; Table 1) and 1060–920 cal yr B.P. (sticks of forest-floor charcoal from a fissure in Crane Lake trench; Table 1).

Although Kelsey et al. (2008) acknowledged that older platform uplift at the west end of the Toe Jam Hill fault scarp on the west coast of Bainbridge Island was known only to predate the Restoration Point earthquake and postdate the time that regional Holocene sea level stabilized (ca. 7 ka), Kelsey et al. (2008) suggested that uplift of the older platforms here and at Point Glover occurred during earthquake C of Nelson et al. (2003a; Figs. 2A and 4). Because none of the older platforms have been dated, they could have been uplifted during either or both of earthquakes B and C, or perhaps during an earlier late Holocene earthquake.

Strong Shaking in the Seattle Fault Zone

Vented sand is a widespread effect of strong shaking during the millennial earthquake series (e.g., Whistler et al., 2002). Martin and Bourgeois (2012) applied stratigraphy and sedimentology to distinguish between sandy beds deposited by tsunamis or through liquefaction venting caused by seismic loading at four of seven previously identified sites in the southern lowland. Thorough work by Martin and Bourgeois (2012) at Lynch Cove (Fig. 1C) led them to reinterpret sandy beds as liquefaction features rather than tsunami deposits, as had been concluded by Hemphill-Haley (1996) and Jovanelly and Moore (2009).

The only long record of strong shaking during Holocene earthquakes in the southern lowland comes from Lake Washington, astride the Seattle fault zone (Figs. 1C and 5). Through study of more than 45 gravity and piston cores, sidescan swath imagery, and high-resolution seismic reflection profiling, Karlin and Abella (1992, 1996) and Karlin et al. (2004) identified 21 widely distributed turbidites, probably induced by strong shaking since 7.6 ka, for an average turbidite recurrence of 300–400 yr.

New Evidence of Surface-Rupturing Earthquakes

IslandWood Scarp on Bainbridge Island

In the Spotted Frog trench on the IslandWood scarp on southern Bainbridge Island (Fig. 2A), till and other ice-contact deposits on Miocene volcaniclastic deposits were twice thrust over a Holocene forest soil developed on the ice-contact deposits (Figs. 2A and 6; Fig. S1 in the Supplemental File [see footnote 1]). Based on displacements of the ice-contact deposits and faulted colluvium from the first earthquake, slip during the first earthquake was <1.7 m and during the second earthquake was >0.9 m (measurements explained in Fig. S1 in the Supplemental File [see footnote 1]). Additional folding during these or possibly earlier earthquakes accounts for the vertical displacement of 3.5 m across the scarp. Two of four ^{14}C ages on detrital charcoal in overridden soil horizons place the earthquakes in the same time frame as earthquakes C and D in the Toe Jam Hill fault trenches (Table S1 in the Supplemental File [see footnote 1]). An age of 1.2 ka (1290–1160 cal yr B.P.; Table 1) on charcoal from a thin AB horizon developed on hanging-wall-collapse colluvium deposited following the first earthquake shows that the second earthquake occurred after earthquake C (Figs. 5 and 6). If the ruptures on the IslandWood scarp coincide with those on the subparallel Toe Jam Hill fault scarp 1.3 km to the south, the first earthquake in the Spotted Frog trench correlates with earthquake C and the second earthquake correlates with earthquake D.

Relation of the Toe Jam Hill Scarp to the Platform on Eastern Bainbridge Island

Bucknam et al. (1999) inferred that because no scarp was observed where the Toe Jam Hill fault intersects the uplifted platform that continues 2 km east to Restoration Point on the east coast of Bainbridge Island, faulting observed in trenches across the scarp must be older than uplift of the platform (Fig. 2A; Sherrod et al., 2000). However, Nelson et al. (2003a) thought it was unlikely that surface faulting on the Toe Jam Hill scarp would not have occurred during the very large Restoration Point earthquake (which they correlated with earthquake D). The scarp rapidly decreases in height from 6 m to <2 m as it approaches a landslide above the heavily forested platform on the east coast of the island (Nelson et al., 2002; Kelsey et al., 2008). A 30-m-long trench south of the projected intersection of the fault with the platform exposed 1–2.5 m of soft, massive marine sand on its surface, but no trace of a scarp was found in or near the trench.

To test for possible vertical offset of the uplifted platform by the fault we measured the platform's shoreline angle (back edge) north and south of the fault where the platform intersects the hillside (Figs. S2 and S3 in the Supplemental File [see footnote 1]). We measured 48 topographic profiles on lidar imagery, parallel with and <200 m north and south of the projection of the Toe Jam Hill scarp, across the platform. We estimated the elevation of the shoreline angle of the platform along each profile by projecting the slope of the platform westward to the hillside. Means of shoreline angle estimates in groups of profiles north and south of the projection of the fault across the platform ($n = 24$ for each group) differed by 1.2 m. A paired t-test on the means rejects the null hypothesis ($p << 0.05$) that there is no difference in the elevation of the shoreline angles on either side of the projected trace of the fault. From this result, we infer that surface faulting displaced the platform during earthquake D, but the <1.5-m-high fault scarp in the soft marine sediment on the platform is too broad or too eroded to now identify.

Scarps and Shorelines of the Point Glover Peninsula

Two east-west–trending fault scarps truncate glacial topography on the Point Glover peninsula ~2 km southwest of the Toe Jam Hill fault scarp (Fig. 2A). The older of the two, the north-facing Point Glover scarp, is ~1 km long and as much as 8 m high (Fig. 4; Nelson et al., 2003b; Kelsey et al., 2008). The younger, steeper Waterman Point scarp is 1.6 km long and 4 m high along its western third and tapers to 1 m high on the uplifted platform on the east side of the peninsula.

Three trenches across the Waterman Point scarp exposed weathered and glacially sheared Blakeley Formation sandstone and mudstone of Oligocene and late Eocene age overlain by till and proglacial lake and fluvial deposits (Figs. 4, 7, 8, and 9). We interpret that bedrock in the Madrone Ridge trench was thrust southward over weathered ice-contact deposits along fault F1 during a first earthquake (Fig. 7C). During

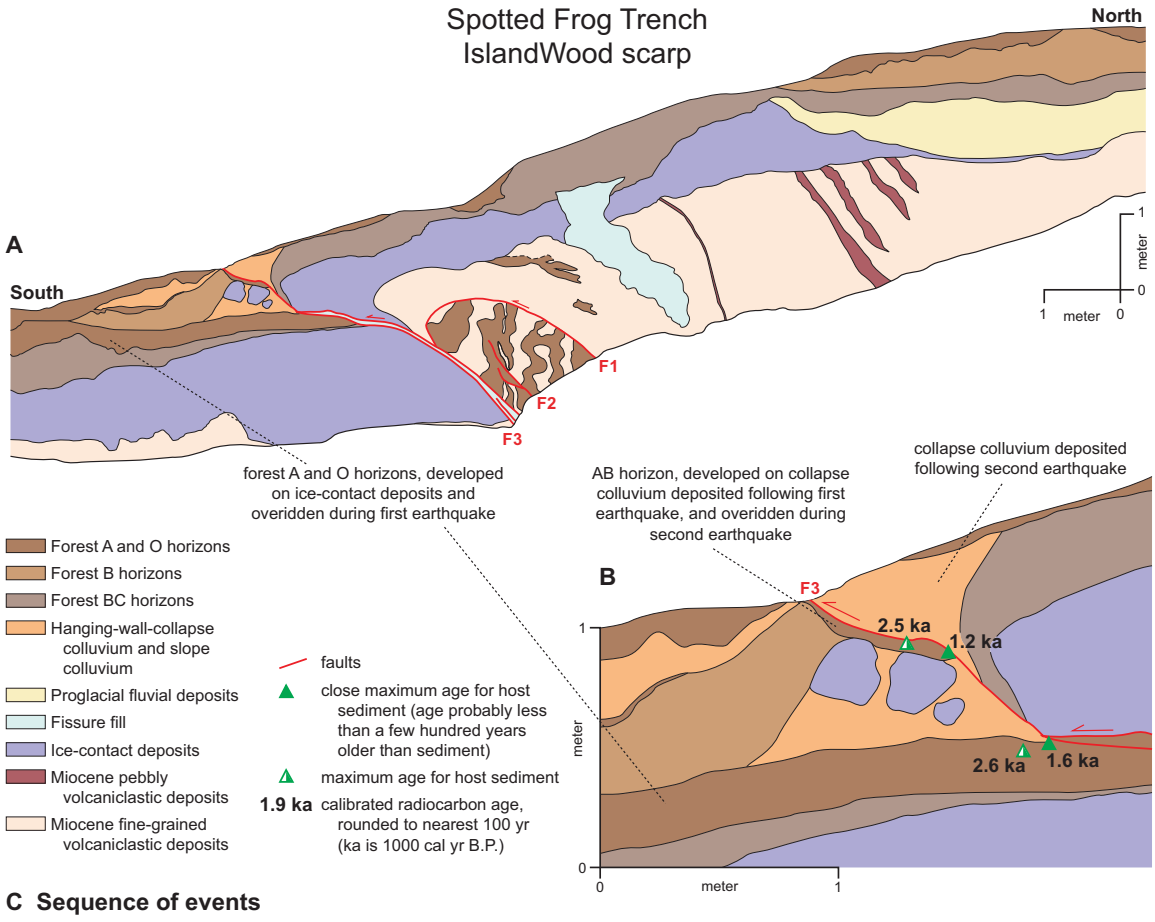

C Sequence of events

1 Advance of the Puget glacial lobe over uplifted, eroded, and weathered volcaniclastic deposits of the Middle Miocene Blakely Harbor Formation (late Pleistocene).
2 Deposition of subglacial ice-contact deposits over bedrock shortly followed by deposition of proglacial fluvial sediment in a small channel (probably 17–16 ka). Because the sediment filling the fissure in the middle of the trench is well consolidated like the adjacent ice-contact deposits, the fissure probably formed during glacial shearing prior to ice retreat rather than during late Holocene faulting.
3 Development of a forest soil (A and AB horizons) with a weak structural B horizon on the ice-contact, proglacial, and fissure fill deposits, followed by extensive root stirring (postglacial through late Holocene).
4 During a first earthquake, about 1.6 m of reverse faulting along fault F3 thrust the hanging wall over the postglacial forest soil developed on the ice-contact deposits. Deformation and slumping of the tip of the hanging wall led to deposition of hanging-wall-collapse colluvium containing blocks of the ice-contact deposits.
5 Continued forest soil development with root stirring on the hanging wall and footwall of the fault scarp and development of a thin forest soil on the deformed colluvium.
6 During a second earthquake, about 0.6 m more slip on fault F3 offset the hanging-wall-collapse colluvium deposited during the first earthquake and the thin soil developed on it. During thrusting, the collapse colluvium in the tip of the new hanging wall was deformed as it rode over the the adjacent collapse colluvium.

Figure 6. Fault scarp stratigraphy, ages, and interpretation for the Spotted Frog trench, IslandWood scarp, Seattle fault zone (see Figs. 1C and 2A). (A) Central two-thirds of the west wall of the Spotted Frog trench. (B) Close-up of stratigraphy near the tip of thrust fault F3 in trench wall shown in A. (C) Sequence of depositional and faulting events in the trench. A photomosaic of the trench log with an explanation of fault slip is in Figure S1 in the Supplemental File (see footnote 1). Brian Sherrod, Harvey Kelsey, and Elizabeth Barnett described, sampled, and interpreted the Spotted Frog trench.

a second earthquake, bedrock was thrust along fault F2, higher in the hanging wall, over soil A horizons and colluvium deposited in response to the first earthquake. Key evidence that requires a two-earthquake interpretation is a forest A horizon, developed on slope colluvium deposited following the first faulting event, which was sheared and/or overridden during the second faulting event. The faulted A horizon developed on scarp colluvium is particularly distinct in a supplemental exposure 2 m west of the mapped trench wall. A forest A horizon of this thickness (8 cm) takes decades to centuries to develop (e.g., Lukac and Godbold, 2011); therefore, the earthquakes occurred at least decades apart. The total vertical separation during both faulting events is <2.4 m, suggesting that the 4.3 m height of the scarp is the result of slip on faults F2, F3, and F4, or other unmapped faults beneath them, during earlier surface-deforming earthquakes (Fig. 7;

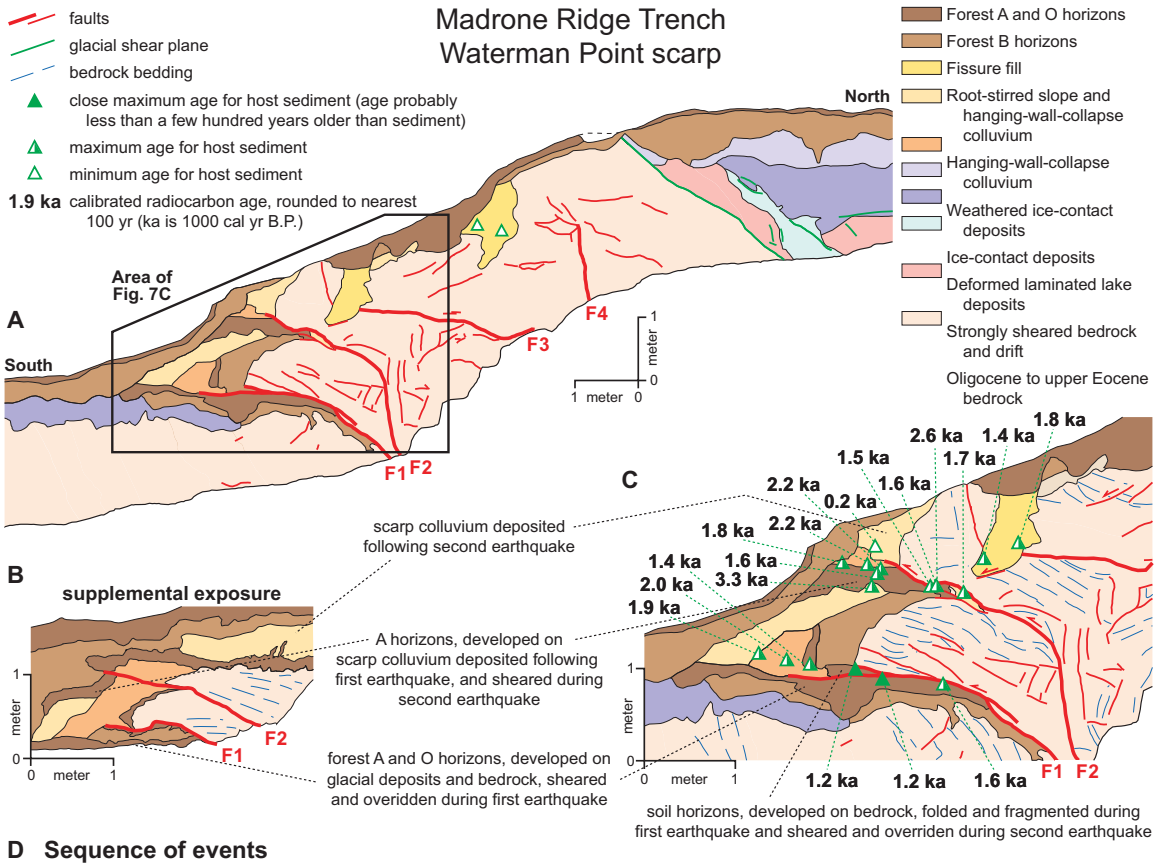

D Sequence of events

1. Advance of the Puget glacial lobe over uplifted, eroded, and weathered Late Eocene to Oligocene turbidite mudstone and sandstone, forming a <1-m-thick subhorizontal zone of glacial shear planes in brecciated bedrock and drift (late Pleistocene).
2. Deposition of ice-contact deposits with locally derived clasts over the zone of sheared bedrock and drift in a proglacial environment (probably 17–16 ka).
3. Development of a forest soil with a thick (0.35 m) structural B horizon on the drift and weathered bedrock, followed by extensive root stirring (postglacial to late Holocene).
4. During a first earthquake, reverse faulting along fault F1 thrust bedrock over the forest soil. Deformation and slumping of the forest soil on bedrock in the hanging wall above F1 rotates the A horizon into a subvertical position (main trench wall on right, above). Fragments of the soil accumulate as hanging-wall-collapse colluvium in a wedge of sediment adjacent to the rotated A horizons. Total slip along F1 is 2.1–2.4 m, with vertical stratigraphic separation about 1.3–1.5 m.
5. Gradual deposition of silty, sandy slope-derived colluvium over the collapse colluvium and rotated A horizons on the F1 hanging wall, followed by continued forest soil development with root stirring on the hanging wall and footwall of the fault scarp and development of a new forest soil on rotated A horizons and overlying slope colluvium.
6. During a second earthquake, reverse faulting primarily along fault F2 thrusts deformed bedrock over the new A horizons and overlying slope colluvium. Sheared blocks of the new forest soil and fragments of the soil accumulate as hanging-wall-collapse colluvium in a wedge of sediment at the tip of F2. Minimum slip along F2 is about 0.8 m.
7. Deposition of a wedge of coarse sandy slope colluvium, derived mostly from bedrock, over the new wedge of collapse colluvium, followed by continued soil development with root stirring on the hanging wall and footwall of the scarp, and by development of a new A horizon on the most recent scarp colluvium.

Figure 7. Fault scarp stratigraphy, ages, and interpretation for the Madrone Ridge trench, Waterman Point scarp, Seattle fault zone (see Figs. 2A and 4). (A) Central two-thirds of the west wall of the Madrone Ridge trench (m6 to m20 on trench wall grid in Nelson et al., 2003b, http://pubs.usgs.gov/mf/2003/mf-2423/). (B, C) Close-up of stratigraphy near faults F1 and F2 in trench wall shown in A, and in a supplemental exposure dug 2 m west and parallel to trench wall. Drawing of supplemental exposure was made from notes and photographs without detailed measurements. (D) Sequence of depositional and faulting events in the trench. Sam Johnson, Koji Okumura, Alan Nelson, Robert Bogar, Brian Sherrod, Ray Wells, Harvey Kelsey, Lee-Ann Bradley, and Yoko Ota described, sampled, and interpreted the Madrone Ridge trench.

slip measurements explained on trench log in Nelson et al., 2003b).

Except for one charcoal age of 0.2 ka in the youngest slope colluvium, which we infer was deposited in a young root cast, the youngest ages (1.2 ka) from the trench are on charcoal in the sheared A horizon beneath the hanging wall of fault F1. These relations show that both surface-rupturing earthquakes are younger than 1290 cal yr B.P. (ages of 1290–1180 cal yr B.P. and 1290–1140 cal yr B.P. in Table 1).

Approximately 100 m west of the Madrone Ridge trench, the Snowberry trench, across a steep, 3.5-m-high scarp, exposed Blakeley Formation that was thrust southward over weathered ice-contact deposits and glacial lake sediment along fault F1 (Figs. 4 and 8). Distinct, overturned blocks of forest soil A, O, and B horizons beneath mudstone and sandstone of the hanging wall suggest that the blocks were plucked from the soil developed on underlying glacial sediments and rotated during thrusting prior to collapse of the thrust tip. The orientations of shear planes within the jumble of rotated blocks of soil, fragments of bedrock, and glacial and root-stirred sediment under the hanging wall suggest rumpling and shearing of the soil and underlying units during a surface-rupturing earthquake. Structural relations in the Snowberry trench do not suggest more than one earthquake.

Four charcoal ages from A and O horizons beneath the hanging wall provide maximum ages for the time of faulting (Fig. 8). The three youngest ages were obtained on samples from a 10-mm-thick seam of charcoal in the O horizon attached to two overturned blocks. Based on excavation and measurement of the charcoal seam in the trench wall, the seam once covered at least 1.7 m^2 of the forest floor. Because it is continuous, undeformed by tree roots, and well preserved, we infer that the seam's wood

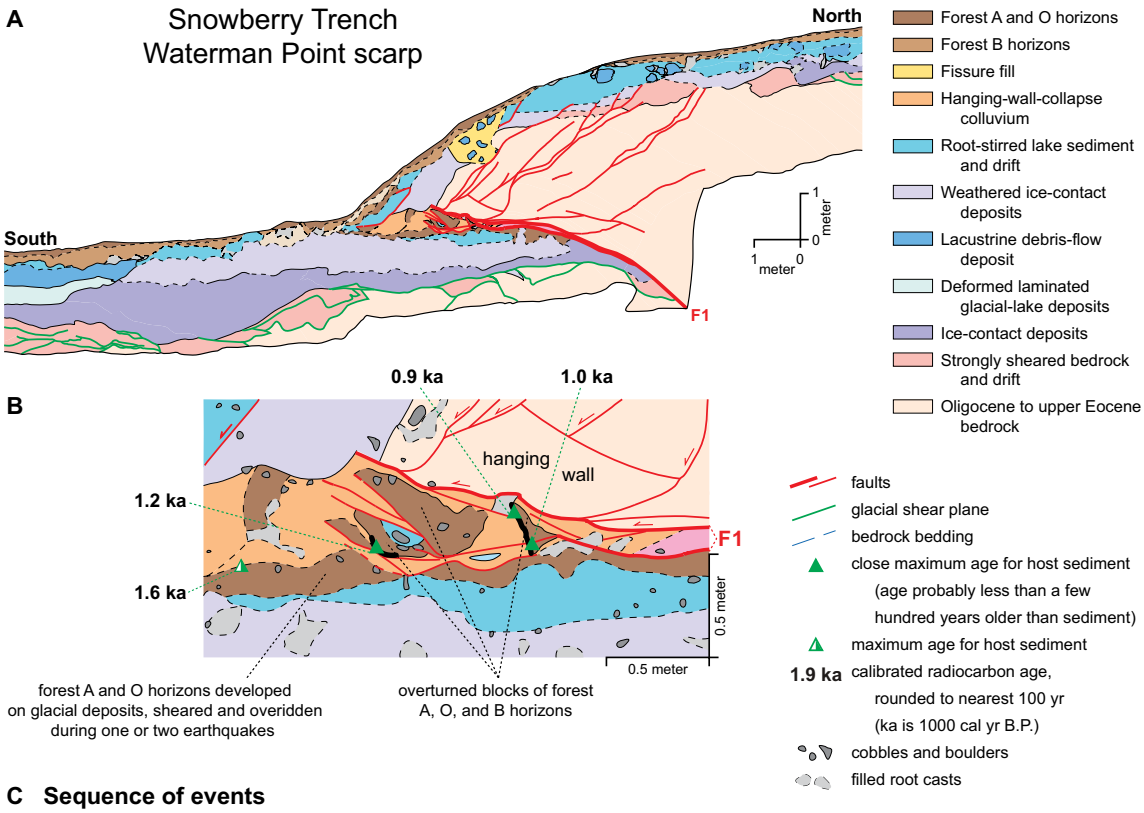

C Sequence of events

1 Advance of the Puget glacial lobe over uplifted, eroded, and weathered Late Eocene to Oligocene turbidite mudstone and sandstone, forming a 1-m-thick subhorizontal zone of glacial shear planes in weathered bedrock and drift (late Pleistocene).
2 Deposition of ice-contact deposits over the shear zone shortly followed by deposition of laminated and debris-flow sediment in a proglacial lake (probably 17–16 ka).
3 Development of a forest soil with a structural B horizon on the lake sediment and drift, followed by extensive root stirring (postglacial through middle Holocene).
4 Reverse faulting slip of 5.3–5.8 m on fault F1, with vertical stratigraphic separation of 3.0–4.3 m, shortly after 980–790 cal yr B.P. (youngest of four ages beneath thrust tip). Based on the stratigraphy in the Madrone Ridge trench, the slip may be the total from two faulting events.
5 Continued forest soil development with root stirring on the hanging wall and footwall of the fault scarp and development of an A horizon on the scarp.

Figure 8. Fault scarp stratigraphy, ages, and interpretation for the Snowberry trench, Waterman Point scarp, Seattle fault zone (see Figs. 2A and 4). (A) Central two-thirds of west wall of Snowberry trench (m6 to m25 on trench wall grid in Nelson et al., 2003b, http://pubs.usgs.gov/mf/2003/mf-2423/). (B) Close-up of stratigraphy near the tip of thrust fault F1 in trench wall shown in A. (C) Sequence of depositional and faulting events in the trench. Alan Nelson, Brian Sherrod, Robert Bogar, Harvey Kelsey, Ray Wells, Sam Johnson, Lee-Ann Bradley, Ian Madin, Steve Personius, Vicki McConnell, Frank Hladky, Michael Polenz, and Mark Molinari described, sampled, and interpreted the trench.

burned <200 yr prior to faulting. Two of the three younger ages (1.2 ka and 1.0 ka; Fig. 8) are consistent with the ages for faulting in the Madrone Ridge trench and the Toe Jam Hill fault trenches, but the third is younger (0.9 ka, age of 980–790 cal yr B.P.; Table 1). In our later analysis of ^{14}C ages, we explain how the youngest age may be evidence for a second surface-rupturing earthquake in the Snowberry trench.

Approximately 600 m east of the Madrone Ridge trench, the Nettle Grove trench exposed Blakeley Formation thrust southward over sheared and weathered ice-contact deposits along faults F1, F2, and F3 during 1 or 2 earthquakes (Figs. 4 and 9). Faults F1, F2, and F3 may have slipped during the same earthquake or during two earthquakes, the first on F1 and F2, and the second on F1 and F3 (Fig. 9C). Total slip measured by stratigraphic separations along the 3 faults is at least 4.0 m. The vertical separation between the hanging wall and footwall is

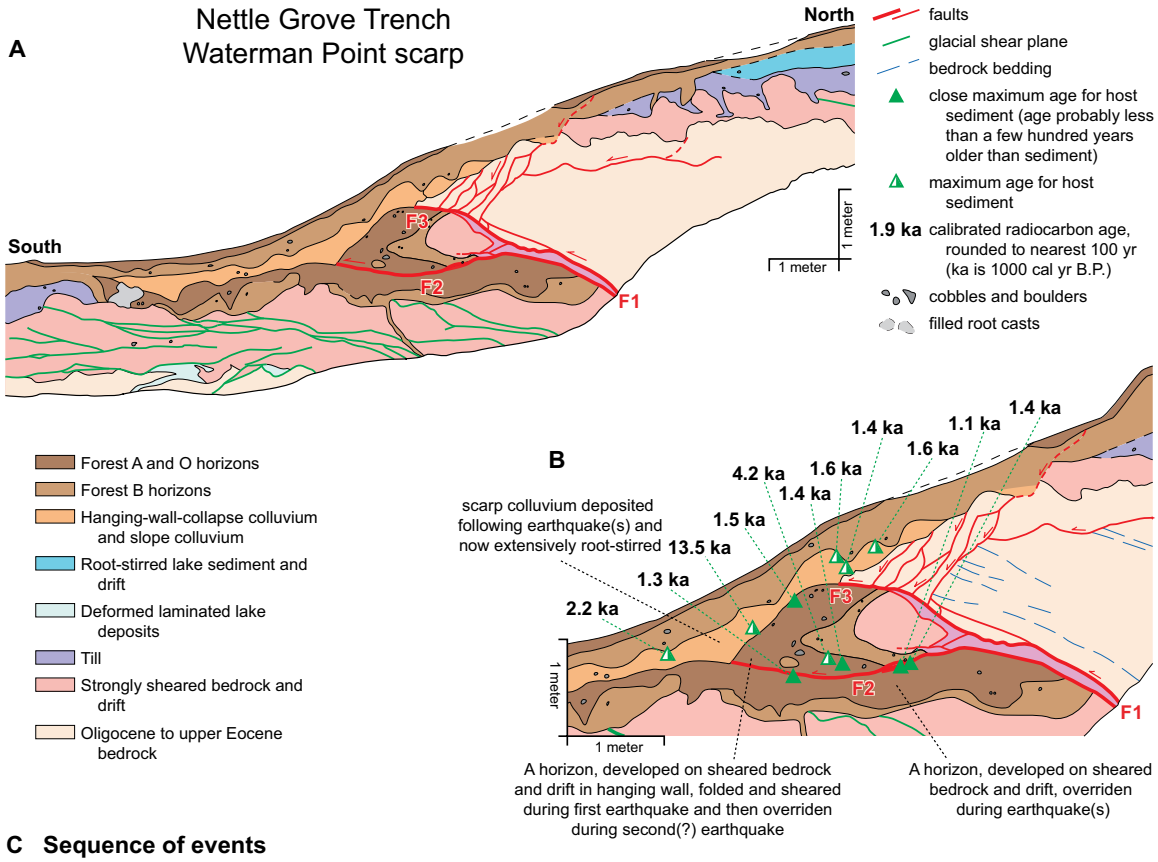

C Sequence of events

1 Advance of the Puget glacial lobe over uplifted, eroded, and weathered Late Eocene to Oligocene turbidite mudstone and sandstone, forming a 0.5-to-1.5-m-thick subhorizontal zone of glacial shear planes in bedrock and drift (late Pleistocene).

2 Deposition of till over the shear zone shortly followed by deposition of sediment in a proglacial lake (probably 17–16 ka).

3 Development of a forest soil with a structural B horizon on the lake sediment and drift, followed by extensive root stirring (postglacial through late Holocene).

4 Because no slope colluvial deposits (which may accumulate gradually between earthquakes) were mapped in the Nettle Grove trench, we are uncertain whether or not faults F2 and F3 slipped during the same earthquake or during separate earthquakes.
If a single earthquake: during the earthquake reverse fault F1 slipped about 2.7 m and the forest soil capping sheared bedrock and drift in the hanging wall was folded and then collapsed, burying the adjacent part of the same undeformed soil just to the south. As fault F1 continued to slip, a new fault (F3) propagated through the folded/collapsed hanging wall, overidding the folded forest soil in the hanging wall. Slip along F3 during this second stage of faulting was a minimum of 1.3 m. Following slip on F3, the overlying bedrock of the hanging wall collapsed in a series of small normal faults near the tip of F3.
If two earthquakes are recorded by the stratigraphy near F2 and F3, then slip during the first earthquake was along F1 and F2 and slip during the second earthquake was along F1 and F3. If slip is the result of two earthquakes, the thin wedge of slope colluvium that was likely deposited following the first earthquake, has probably been incorporated by root stirring into the long, thin deposit of slope colluvium in the trench.

5 Continued forest soil development with root stirring on the hanging wall and footwall of the fault scarp, and by development of a new forest A horizon on the scarp colluvium.

Figure 9. Fault scarp stratigraphy, ages, and interpretation for the Nettle Grove trench, Waterman Point scarp, Seattle fault zone (see Figs. 2A and 4). (A) Central two-thirds of west wall of Nettle Grove trench (m5 to m15 on trench wall grid in Nelson et al., 2003b, http://pubs.usgs.gov/mf/2003/mf-2423/). (B) Close-up of stratigraphy near faults F1, F2, and F3 in trench wall shown in A. (C) Sequence of depositional and faulting events in the trench. Harvey Kelsey, Ray Wells, Koji Okumura, Robert Bogar, Brian Sherrod, Alan Nelson, and Lee-Ann Bradley described, sampled, and interpreted the trench.

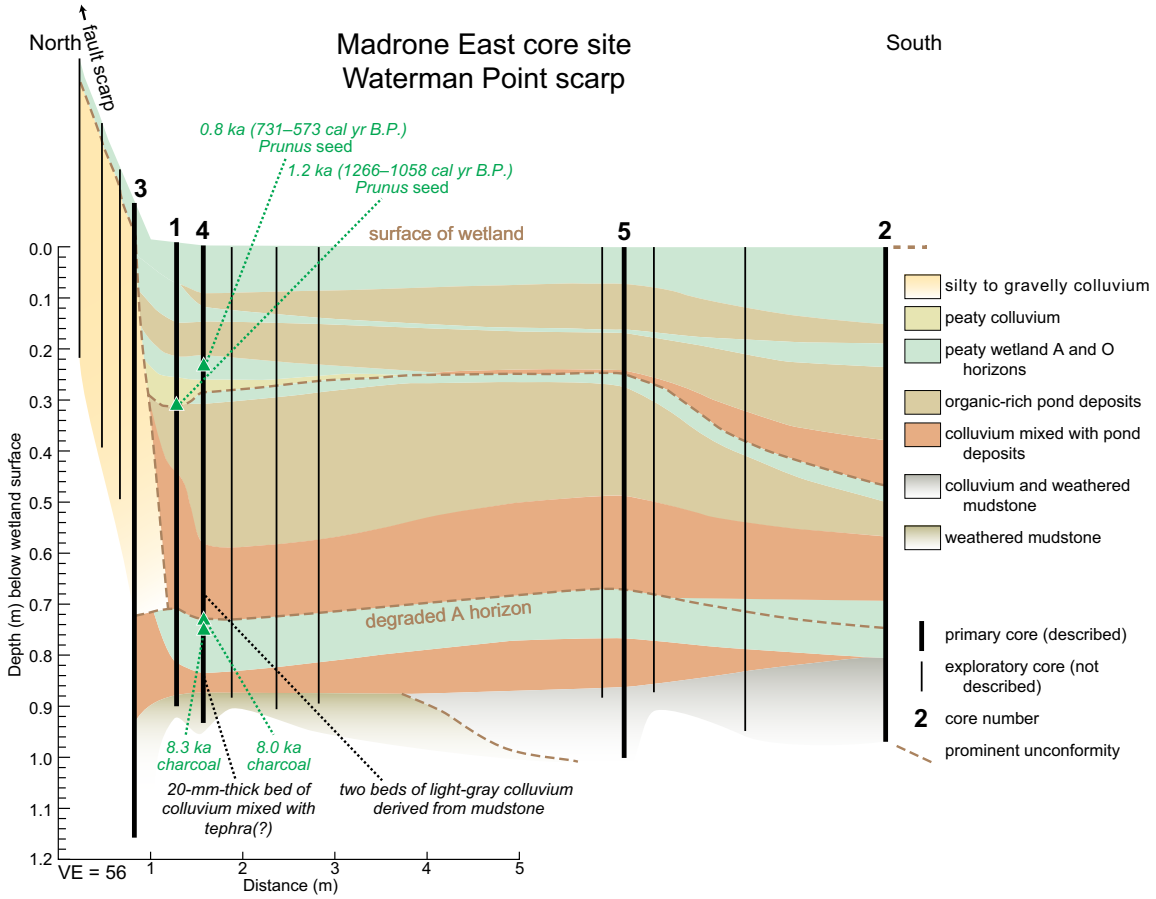

Figure 10. Cross section based on stratigraphy in 15 2.5-cm-diameter gouge cores extending south from the base of the Waterman Point fault scarp ~70 m east of the Madrone Ridge trench (see Figs. 2A and 4; location on high-resolution lidar [light detection and ranging] imagery in Nelson et al., 2003b, http://pubs.usgs.gov/mf/2003/mf-2423/). Location of section and descriptions of five cores are shown in Figure S4 in the Supplemental File (see footnote 1). VE—vertical exaggeration.

3.5–3.7 m, whereas surface displacement measured across the scarp is ~3.2 m (slip measurements explained on trench log in Nelson et al., 2003b). The youngest sampled charcoal in the trench (1.1 ka; Fig. 9) was found in the sheared A horizon beneath the hanging wall and fault F2. The age (1180–1010 cal yr B.P.; Table 1) is a maximum age for surface rupture at this site.

Thus, based on stratigraphy in the 3 trenches along a 700 m section of the Waterman Point scarp, interpretations range from 1 very large surface-rupturing earthquake to 2 large surface-rupturing earthquakes in the past 1300 yr. We infer the history of surface ruptures to be the same over such a short section of scarp and conclude that the stratigraphy exposed in the Madrone Ridge trench is more complete than that in the other two trenches. The vertical component of slip measured for each of the faulting events in the trenches compared with the height of the scarp also suggests that the scarp records multiple earthquakes.

To test the two-earthquake interpretation, we described and dated wetland stratigraphy at two sites adjacent to the Waterman Point scarp (Fig. 4; scarp map on lidar imagery with 1 m contours in Nelson et al., 2003b). Approximately 70 m east of the Madrone Ridge trench, the stream channel in a 14-m-wide valley cut into the scarp is vertically displaced ~0.5–1.0 m. A cross section with 15 gouge cores extending south from the base of the fault scarp at the valley mouth shows that sediment of the past 8000 yr is <1 m thick (Madrone East core site, Fig. 10; Fig. S4 in the Supplemental File [see footnote 1] shows core descriptions with sketch map). Colluvium with fragments of peat derived from the scarp in cores 1 and 4, overlying the younger of two wetland O horizons developed on sediment ponded against the scarp, is bracketed by ages on *Prunus*-type seeds between 1.2 and 0.7 ka (Table 1). The ages suggest that the colluvium, probably deposited in response to faulting along the scarp, dates from the time of the two earthquakes inferred from the Madrone Ridge trench (and the 1–2 earthquakes recorded in the Snowberry and Nettle Grove trenches; Figs. 7–9).

At the Wataugua Beach core site, ~140 m east of the Nettle Grove trench site, we found evidence consistent with a two-earthquake interpretation. A composite stratigraphic section with ^{14}C ages compiled from 6 gouge cores 1–2 m south of the scarp-wetland contact (Figs. 4 and 11; Fig. S5 in the Supplemental File [see footnote 1] shows composite section description with sketch map) shows two beds of probable colluvium (units 5–7 and 10) separated by 0.24 m of peat and peaty mud (units 8 and 9). Radiocarbon ages on a twig from the top of unit 4 (0.8 ka) and from a fragile herb bract or bud from the upper contact of pond deposits mixed with the colluvium (unit 7; 0.9 ka) are consistent with the colluvium (units 5–7) having been deposited in a pond along the scarp shortly following an earthquake of the millennial series (Fig. 12). Flat-lying *Pseudotsuga menziesii* needles from the upper 10 mm of peat

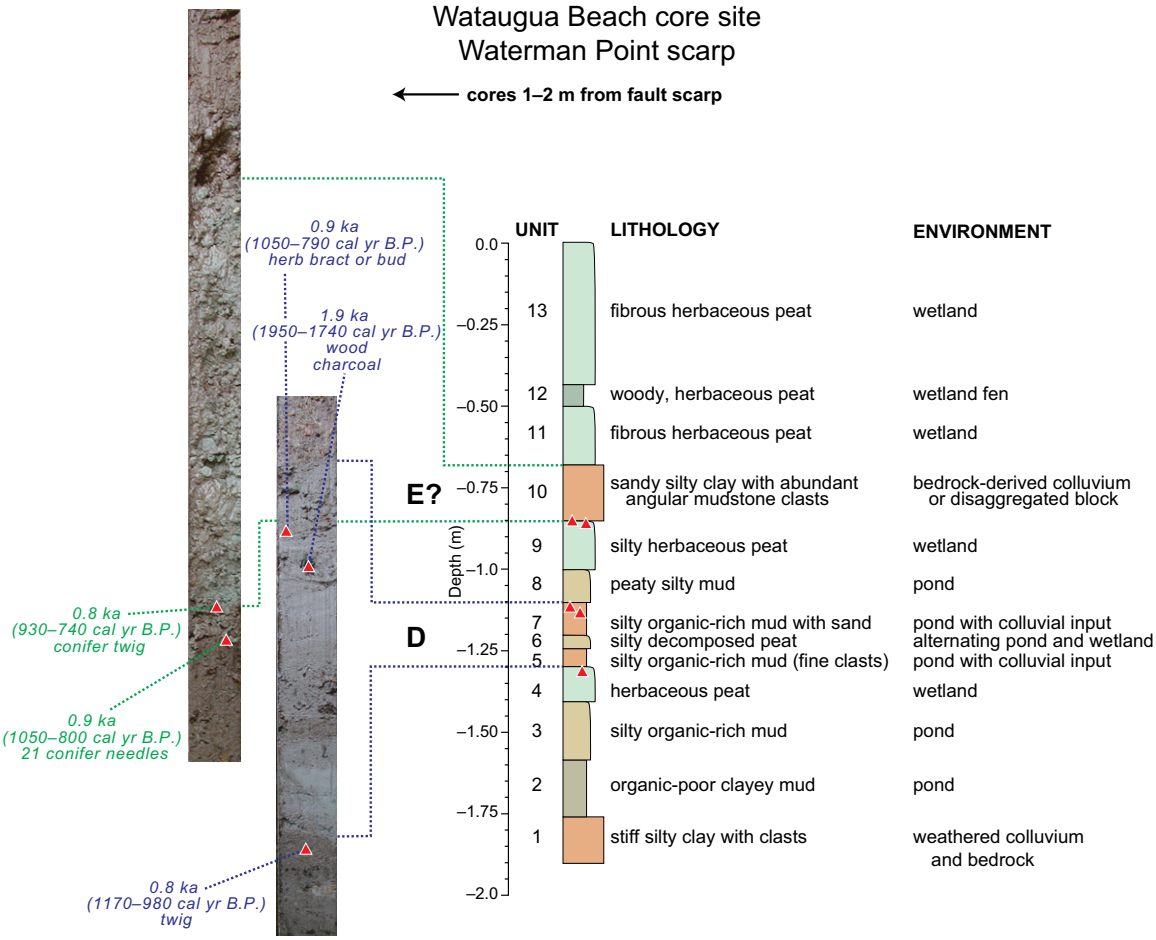

Figure 11. Composite stratigraphic section compiled from six gouge cores within 2 m of each other at the Wataugua Beach core site, 140 m east of the Nettle Grove trench site (see Figs. 2A and 4; location on high-resolution lidar [light detection and ranging] imagery in Nelson et al., 2003b, http://pubs.usgs.gov/mf/2003/mf-2423/). Units within the composite section are numbered from 1 to 13. Location of section and descriptions of cores are in Figure S5 in the Supplemental File (see footnote 1).

beneath the upper scarp colluvium 0.25 m higher in the section (unit 9) gave a similar age (0.9 ka), but a *Pseudotsuga*-type twig (petiole with distinct pegs) at the upper unit 9 contact 20 mm above the needles yielded an age ~100 yr younger (0.8 ka, Fig. 11; 930–740 cal yr B.P., Table 1). Typical rates of deposition for peat and pond sediments in such a small wetland basin (less than a few mm/yr) suggest that 0.24 m of peat and pond deposits between units 7 and 10 took decades to accumulate. Although bedrock-derived unit 10 may be the disaggregated remains of a block of hanging-wall bedrock that rolled down the scarp decades after the first surface-rupturing earthquake, we infer that it is slope colluvium deposited in response to a second surface-rupturing earthquake. Site proximity and similar ^{14}C ages suggest that the two possible earthquakes identified in the Wataugua Beach cores are the 2 surface-rupturing earthquakes identified in the Madrone Ridge trench, 140 m to the west.

Remnants of uplifted shoreline platforms north of the Waterman Point fault scarp are additional evidence consistent with a history of at least three late Holocene earthquakes on the Waterman Point and Point Glover faults. The continuous 8–10-m-high platform, which extends around both sides of the Point Glover peninsula, shows >6 m of uplift of this part of the hanging wall of the master Seattle thrust during the Restoration Point earthquake (Fig. 4; Bucknam et al., 1992; Sherrod et al., 2000; Kelsey et al., 2008). Two <50-m-wide remnants of a platform 70–200 m north of the Waterman Point fault and 2–3 m above the continuous platform may mark an earlier episode of uplift of the hanging wall of the fault during a pre–Restoration Point earthquake. These remnants are several meters lower than the platform at the northern tip of the peninsula uplifted during faulting on the Point Glover fault (Fig. 4), which also predates the Restoration Point earthquake (Kelsey et al., 2008). We also mapped remnants of a third, lowest shoreline platform 200 m southeast and 370 m northeast of Waterman Point (Fig. 4) at an elevation of ~2 m, ~4 m below the platform of the Restoration Point earthquake. These smaller remnants (<30 m wide and <50 m long) are consistent with 1–2 m of uplift north of the Waterman Point scarp during the younger surface-rupturing earthquake identified in the Madrone Ridge trench. They also match our interpretation of earthquake-induced deposition of the younger colluvium at the Wataugua Beach core site.

Earthquake Correlation and Timing in the Central Seattle Fault Zone

Selection and Analysis of ^{14}C Ages

To correlate earthquakes from site to site and to make more precise estimates of the times of surface-deforming earthquakes, we reevaluated

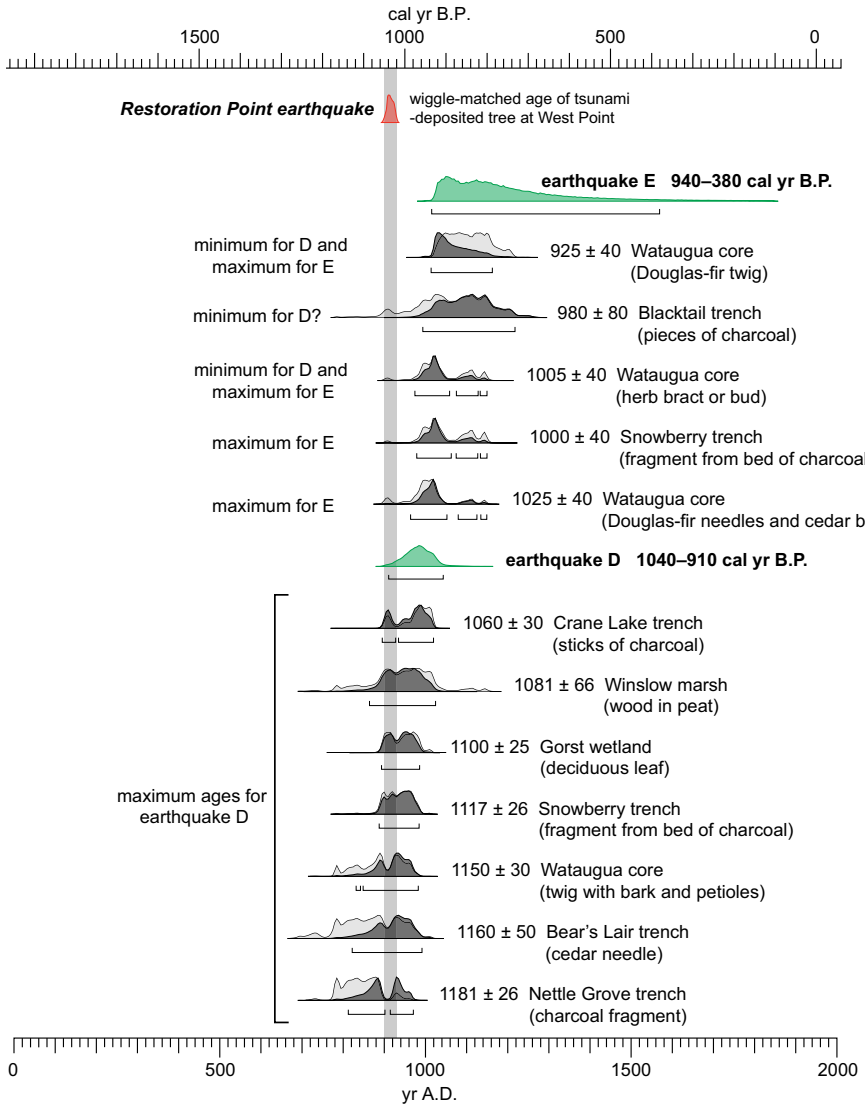

Figure 12. Example of how probability distributions for the times of earthquakes (shown in green) in Figure 5 are calculated using maximum and minimum limiting ^{14}C ages (listed in Table 1) with the program OxCal (version 4.1; Bronk Ramsey, 1995, 2009) and the ^{14}C calibration data set of Reimer et al. (2009). Based on our correlation of earthquake D of Nelson et al. (2003a) on the Toe Jam Hill fault with the older of the two earthquakes on the Waterman Point fault, we selected the most closely limiting maximum and minimum ages for earthquake D (sites discussed in text) as labeled in the figure. The gray distribution for each age is the original probability distribution for each calibrated age. Black distributions show how distributions shift as a result of the OxCal analysis. Seven ages from correlated sites are close maximum ages for earthquake D. Based on stratigraphic position, two ages are minimum ages for earthquake D and also maximum ages for earthquake E on the Waterman Point fault. The age from the Blacktail trench is a minimum age for earthquake D only if the dated charcoal in scarp colluvium was deposited in response to scarp folding during earthquake D; because the charcoal is detrital, it could be older than its host sediment. Two other ages are close maximum ages for earthquake E. To illustrate this interpretation of the timing of earthquake E, we used OxCal to calculate a skewed probability distribution (see text).

the stratigraphic context and types of materials dated for ~260 ^{14}C ages from paleoseismic sites in the southern Puget Lowland. For each dated sample, we considered the sample stratigraphic and geomorphic context, composition, size, weight, probable source, condition (e.g., decayed, abraded), potential for contamination with younger or older material, potential for being reworked or introduced from a younger horizon (e.g., burned roots), and consistency with other ages at the sample's site and correlative sites (e.g., Nelson et al., 2003a; Bird, 2007; Kemp et al., 2013). For published studies we mostly made the same site-to-site correlations of earthquakes as made by the original investigators (e.g., Sherrod, 2001; Nelson et al., 2003a; Sherrod et al., 2004a). Of the 214 ages that place some constraint on the times of earthquakes (Table S1 in the Supplemental File [see footnote 1]), we selected increasingly smaller subsets of ages based on higher sample quality, more stratigraphically consistent ages, and more closely limiting inferred maximum or minimum ages on the times of earthquakes (Table 1). In most cases, we assumed the youngest of detrital ages from faulted or folded deposits to be the most closely limiting maximum age of an earthquake. As explained earlier and in Figure 12, however, we relied on stratigraphic context to infer that six of the detrital charcoal ages are probably minimum ages for earthquakes (Table 1). Following many previous paleoseismic studies (e.g., Fumal et al., 2002; Atwater et al., 2004; Lienkaemper and Williams, 2007; Fraser et al., 2010; DuRoss et al., 2011; Berryman et al., 2012), we then used Bayesian methods (Bronk Ramsey, 1995, 2009; Biasi and Weldon, 2009; Lienkaemper and Bronk Ramsey, 2009) to calculate a probability distribution for the times between our selected youngest maximum ages and oldest minimum ages (ages in bold in Table 1; Figs. 5 and 12; Table S2 in the Supplemental File [see footnote 1] lists OxCal program code). Although we use the OxCal-modeled probability distributions to correlate and date earthquakes, the error ranges of the distributions may not encompass all uncertainties in the times of earthquakes. For example, the distributions do not include additional types of sample context error, such as the residence time of charcoal on a forest floor (Gavin, 2001; Nelson et al., 2003a), because we have no way of accurately estimating them.

Earthquakes on Bainbridge Island and Point Glover Peninsula

Limiting ages from the Crane Lake and Mossy Lane trenches on the Toe Jam Hill fault place earthquakes B and C of Nelson et al. (2003a) within intervals (2σ ranges of OxCal-modeled

probability distributions) of 2650–1940 cal yr B.P. and 1350–1170 cal yr B.P., respectively (Fig. 5). If the youngest charcoal age from the Spotted Frog trench on the IslandWood scarp closely limits the time of the second faulting event in that trench (Fig. 6), then the first faulting event probably records earthquake C. The older shoreline platforms studied by Kelsey et al. (2008) may correlate with earthquakes B and/or C. Sherrod et al. (2000) listed coseismic uplift during several moderate magnitude earthquakes as one of three possible explanations for salinity changes dated to 3.5–2.5 ka in a sparsely sampled section of core from the Restoration Point marsh (Fig. 2A). Kelsey et al. (2008, p. 1595) considered these events as "a cluster of ~2–3 folding (local) earthquakes."

We follow Kelsey et al. (2008) in inferring that the Toe Jam Hill and the Waterman Point faults, the east-west trends of which are offset <1 km (Fig. 2A), ruptured during the same earthquake, most likely the Restoration Point earthquake. Our correlation of earthquakes between the two faults suggests, however, that both faults do not always rupture during the same earthquakes. Nelson et al. (2003a) attributed the youngest surface-rupturing event in the Toe Jam Hill fault trenches (earthquake D) to the Restoration Point earthquake, citing ^{14}C ages and the greater slip exposed in trenches during that earthquake than for earlier earthquakes. In contrast, our dating of two colluviums (units 5–7 and 10; Fig. 11) in wetland cores along the Waterman Point scarp suggests that the older of the two faulting events on that scarp most likely correlates with the Restoration Point earthquake. An age on a conifer twig (930–740 cal yr B.P.; Fig. 12) from the top of the peat (unit 9) that separates the colluviums is ~100 yr younger than the most precise age for the Restoration Point earthquake (1050–1020 cal yr B.P.; Figs. 5 and 12). Of course, the dating cannot preclude separate rupture of these scarps during other moderate to large earthquakes of the millennial series.

If, as we infer above, the unit 10 colluvium correlates with the second faulting event in the Madrone Ridge trench and with the second of the two possible faulting events in the Nettle Grove trench, then a younger surface rupture (earthquake E) broke the Waterman Point scarp at least decades after earthquake D in the Toe Jam Hill fault trenches. We infer this rupture to record the Restoration Point earthquake (Fig. 5). Trench mapping identified only one large surface-rupturing event in the Snowberry trench 100 m west of the two-event Madrone Ridge trench, but our OxCal analysis of limiting ages for earthquake D from the Toe Jam Hill fault suggests that the youngest age from the Snowberry trench may be a maximum age for earthquake E (Fig. 12) and possibly a minimum age for earthquake D. The age (980–790 cal yr B.P.) on wood charcoal in a layer of charcoal at the top of an overturned block of forest soil in the fault zone (Fig. 8) is too young (at 2σ) to date forest-floor charcoal incorporated into the fault zone during the Restoration Point earthquake (1050–1020 cal yr B.P.; Fig. 12). If the age is a minimum for earthquake D, then part of the slip along fault F1 in the Snowberry trench occurred during a second earthquake that is younger than earthquake D. An alternative statistical possibility is that the true age of the charcoal is within the youngest tail of its 3σ age distribution, in which case it might still provide a close maximum age for earthquake D.

Because we cannot distinguish between these two alternatives, we use the youngest Snowberry trench age with three other ages from the Wataugua Beach cores only to set an older limit for the time of earthquake E (Fig. 12). As we have no minimum ages for earthquake E, our full interval extends to A.D. 1851, when European settlers arrived in southern Puget Sound. Because we interpret our limiting ages as being close maximums, we use the Zero Boundary command in OxCal to skew the probability distribution for earthquake E toward its older end (methods of Bronk Ramsey, 2008, 2009; as explained by DuRoss et al., 2011). The skewed distribution (940–380 cal yr B.P. at 2σ) best represents our interpretation of the time of earthquake E.

HOLOCENE DEFORMATION IN THE TACOMA FAULT ZONE

In a series of stratigraphic, ^{14}C dating, and paleoecologic studies, Bucknam et al. (1992), Sherrod (2001), Sherrod et al., (2004a, 2004b), and Arcos (2012) identified evidence of substantial late Holocene uplift and subsidence at 12 sites over much of the region of the Tacoma fault zone (Figs. 1C and 2B). Differences in wetland plant fossils and diatom assemblages across uplift and subsidence contacts indicate >1 m of vertical deformation at most sites. Overall, dating at five of the uplift sites and six of the subsidence sites constrains Tacoma fault zone deformation to the millennial earthquake series (1180–790 cal yr B.P.; Sherrod et al., 2004a). Ages that best constrain the time of shoreline deformation include leaf bases of *Triglochin maritima* that limit the uplift of the tide flat on the hanging wall of the fault (Lynch Cove; Fig. 2B) to shortly before 1170–960 cal yr B.P., and the ^{14}C-wiggle-matched age of 1090–1010 cal yr B.P. on rings from a *Pseudotsuga menziesii* stump killed by earthquake subsidence at the Nisqually delta 25 km south of the fault (Red Salmon Creek; Figs. 2B and 5; Table 1).

The >1–3 m of subsidence measured at Little Skookum Inlet led Sherrod (2001; Fig. 1C) to speculate that this subsidence was the result of 2 earthquakes. Following such reasoning, an age of 970–760 cal yr B.P. on the outermost rings of a *Pseudotsuga menziesii* stump in growth position on the modern tide flat at Wollochet Bay postdates the most precise age for the Restoration Point earthquake (1050–1020 cal yr B.P.). Perhaps it records subsidence during a later earthquake or a stress-relaxation response of the crust to the Restoration Point earthquake decades after it (Sherrod et al., 2004b; Table 1).

Catfish Lake Scarps and Related Shorelines

The Catfish Lake fault scarps, which truncate drumlins and outwash channels on the hanging wall of the Tacoma fault (Figs. 1C and 2B), formed in the late Holocene. These linear, 1–6-m-high scarps extend 4.4 km east-west between Hood Canal and Case Inlet (Sherrod et al., 2004a, 2004b; Logan and Walsh, 2007; Nelson et al., 2008, sheet 1) and probably another 2 km to the east beneath Case Inlet (Figs. 1C and 2B; Johnson et al., 2004b; Clement et al., 2010). Seismic reflection profiling east of Allyn shows that the water bottom of Case Inlet on trend with the scarp is warped upward ~2 m, suggesting Holocene growth of a fold above a blind thrust (Johnson et al., 2004b; Clement et al., 2010). The Blueberry trench across the western scarp showed probable late Holocene faulting of a B/E soil horizon developed on weathered till (Sherrod et al., 2004a, fig. 3D therein, 2004b). Reverse separation along at least 2 of 4 small faults offsets the top of the horizon <0.3 m. Although some folding in the till may have a glacial origin, the sharp truncation of the glacial ridges by the scarp at the trench site shows that the scarp formed after the retreat of the Puget ice lobe (later than 16 ka).

In the more recent Cedars trench, across a 6-m-high scarp 0.8 km east of the Blueberry trench (Fig. 2B), we exposed a 30-m-long section of subglacial, ice-contact, and proglacial deposits (Fig. S6 in the Supplemental File [see footnote 1]; trench log in Nelson et al., 2008, sheet 2). Bedding contacts along most of the trench are subparallel to the scarp, indicating that scarp folding is postglacial. Several lines of evidence show that a strongly folded syncline of subglacial or proglacial stream and lake deposits near the base of the scarp predates the retreat of the Puget lobe. Tight folds, truncation surfaces, boudins, and flame structures in lake beds of the syncline are evidence for subaqueous soft-sediment loading and flow. The onlap of its successive lake beds also shows that folding of the syncline was contemporaneous with deposition. A thermoluminescence

age of 110–119 ka on silt-sized feldspar from one of the lake beds shows that synclinal folding considerably predates the last glacial maximum. The syncline axis is strongly oblique to the scarp trend, suggesting that the scarp is much younger than the syncline.

Near the crest of the scarp in the Cedars trench, parallel-bedded sand, deposited in a stream channel cut into the glacial deposits, contains angular, horizontally bedded, fragments of wood charcoal as young as 4.3 ka (Table S1 in the Supplemental File [see footnote 1]). The channel position near the crest of the scarp and the tilt of its bedding parallel with the scarp surface show that the stream could only have deposited the sand prior to scarp folding, and therefore that the scarp formed after 4.3 ka.

At least some of the uplift and folding along the Catfish Lake scarps probably occurred during the millennial earthquake series. An uplifted shoreline north of where the trend of the scarp intersects the western shore of Case Inlet is 4 m higher than its modern tide-flat equivalent south of the scarp south of Allyn (Sherrod et al., 2004a, fig. 2B therein). Stratigraphy beneath a marsh south of Allyn shows that a freshwater swamp developed on the tide flat following the most recent uplift. Seeds from the base of the swamp O horizon give a minimum limiting age for the uplift of 1060–830 cal yr B.P. (Sherrod et al., 2004b; Table 1), an age within the 1180–790 cal yr B.P. interval determined for Tacoma fault zone deformation by Sherrod et al., (2004a). In Catfish Lake and Mill Pond to the west of Allyn, Logan and Walsh (2007) dated the stumps of trees probably killed by lake water impounded during uplift of the scarp. Because the outer rings of the stumps have been eroded, the youngest of the stump ages (1180–940 cal yr B.P.; Table 1) is older than the uplift.

Stansberry Lake Scarps

Near Stansberry Lake ~6 km east of Allyn, a 1-m-high, 1.2-km-long, northwest-trending scarp offsets a 1.7-km-long, 4–12-m-high, east-northeast-trending scarp in the hanging wall of the Tacoma fault (Figs. 2B and 13; Sherrod et al., 2004a, 2004b, fig. 3B therein; see lidar figures in Nelson et al., 2008, sheet 2). Only the younger scarp is tectonic. Our thorough study of a 30-m-long trench across the older scarp, which exposed subglacial ice-contact and fluvial deposits, proglacial fluvial deposits, and overlying root-stirred colluvium, showed no sign of faulting or folding. Erosional unconformities cut on the glaciofluvial deposits beneath the upper half of the older scarp suggest that this gently sloping scarp is the margin of a wide proglacial channel, the opposite margin of which has apparently been eroded (Owl trench log in Nelson et al., 2008, sheet 2).

The Micah trench across the younger scarp exposed three zones of mostly subvertical faults that offset proglacial ice-contact and well-stratified fluvial deposits (Fig. 13; Nelson et al., 2008, sheet 2). Many of the faults trend near 330°, and the upper tips of strands in fault zones 2 and 3 extend upward into recently root-stirred sediment in the lower part of the modern forest soil. Strand tips in fault zone 1 did not extend into root-stirred sediment. However, because such strands are unreliable indicators of the relative age of slip on oblique-slip faults, we conclude that the faulting occurred during a single, probably late Holocene, earthquake. The maximum age of the earthquake is constrained by the youngest of six ages (1530–1400 cal yr B.P.; Table 1) on wood charcoal in the B horizon buried by a wedge of colluvium formed from collapse of the 0.4-m-high fault scarp in fault zone 2. The mean of three ages, from a tree root that grew following deposition of the colluvium, dates the earthquake at prior to 1060–960 cal yr B.P., a time interval within the millennial earthquake series.

Right-lateral horizontal separation of sand lenses in proglacial deposits and a flower-structure–like pattern of faults in fault zone 2 (particularly on the shorter of the two trench walls shown in Nelson et al., 2008, sheet 2) suggest significant lateral slip on the faults. However, the only distinct bedding in the proglacial units offset by the faults is horizontal, preventing measurement of the ratio of vertical to lateral slip. Total oblique slip on the faults may be several times the 0.6 m net vertical displacement across the three fault zones in the trench. Because the young scarp trends at a 60° angle to the trend of the surface projection of the main Tacoma fault in this area (170°), it probably records slip on a short, shallow fault in the hanging wall of the main fault probably caused by folding of the hanging wall. Clement et al. (2010) inferred that the small postglacial faults they imaged 7 km southeast of the Stansberry Lake scarps were either shallowly rooted, bending moment faults produced during folding of the northwest-trending monocline along this part of the Tacoma fault zone, or short strike-slip faults accommodating lateral movement parallel with the monocline. The latter origin is consistent with our oblique-slip interpretation of the faults in the Micah trench.

Sunset Beach Scarps

Complex sets of scarps trend northeast for 3.5 km from Hood Canal (Figs. 1C and 2B; lidar figures in Nelson et al., 2008, sheet 3; Polenz et al., 2009), 1–2 km south of the uplift and liquefaction site at Lynch Cove (Bucknam et al., 1992; Sherrod et al., 2004b; Martin and Bourgeois, 2012), and 6–7 km north of the Catfish Lake scarps. Their shore-parallel position and arcuate morphology suggest many of the larger scarps in the steep bluffs along Hood Canal are landslide head scarps. However, most of the scarps on the glaciated upland south of Hood Canal and trending to the northeast away from the landslide complex are probably tectonic rather than landslide scarps. Landslides with headscarps with the orientation and position of those near the northeast end of the upland scarps would require slide planes of exceptionally low angles. From the slight up-to-the-south displacement of reflectors at 100–200 m depth on a seismic reflection profile that crosses the scarps near their northeast end (Nelson et al., 2008, fig. 13 therein), we infer that the upland scarps formed in response to slip on a south-dipping reverse fault in the underlying Tertiary bedrock, or on a larger north-dipping reverse fault ~1 km to the south. Reflectors suggesting a gently dipping slide plane, as would be expected from a low-angle landslide, are absent on the profiles. Hummocky morphology characteristic of a bulging landslide toe is also not present where it would be expected near the shore of Hood Canal at Lynch Cove (Fig. 1C).

Near the northeast end of the upland scarps, we also dug 2 trenches, ~12 m long, which exposed steeply dipping normal faults in subglacial ice-contact deposits and overlying proglacial fluvial deposits on either side of a 60–80-m-wide graben (Fig. 14). In each of the two trenches on either side of the graben, the youngest dated fragments of detrital charcoal in the scarp-derived colluvium date the normal faulting to younger than 1290–1080 cal yr B.P. (Table 1; Fig. 14), a limiting age that places the time of faulting within the millennial earthquake series. We infer that the Sunset Beach fault scarps, as well as many of the landslide head scarps along Hood Canal (Sarikhan et al., 2007), formed or increased in height during the millennial earthquake series.

Earthquake Timing in the Tacoma Fault Zone

We used OxCal (methods of Fig. 12) with the 12 closest maximum and minimum limiting ages from Tacoma fault zone sites (Table 1) to calculate a fault-wide probability distribution for the time interval of the millennial earthquake series (Fig. 5). This calculation assumes that deformation at all the sites records the same very large earthquake or a cluster of large earthquakes in the span of a few decades (Sherrod

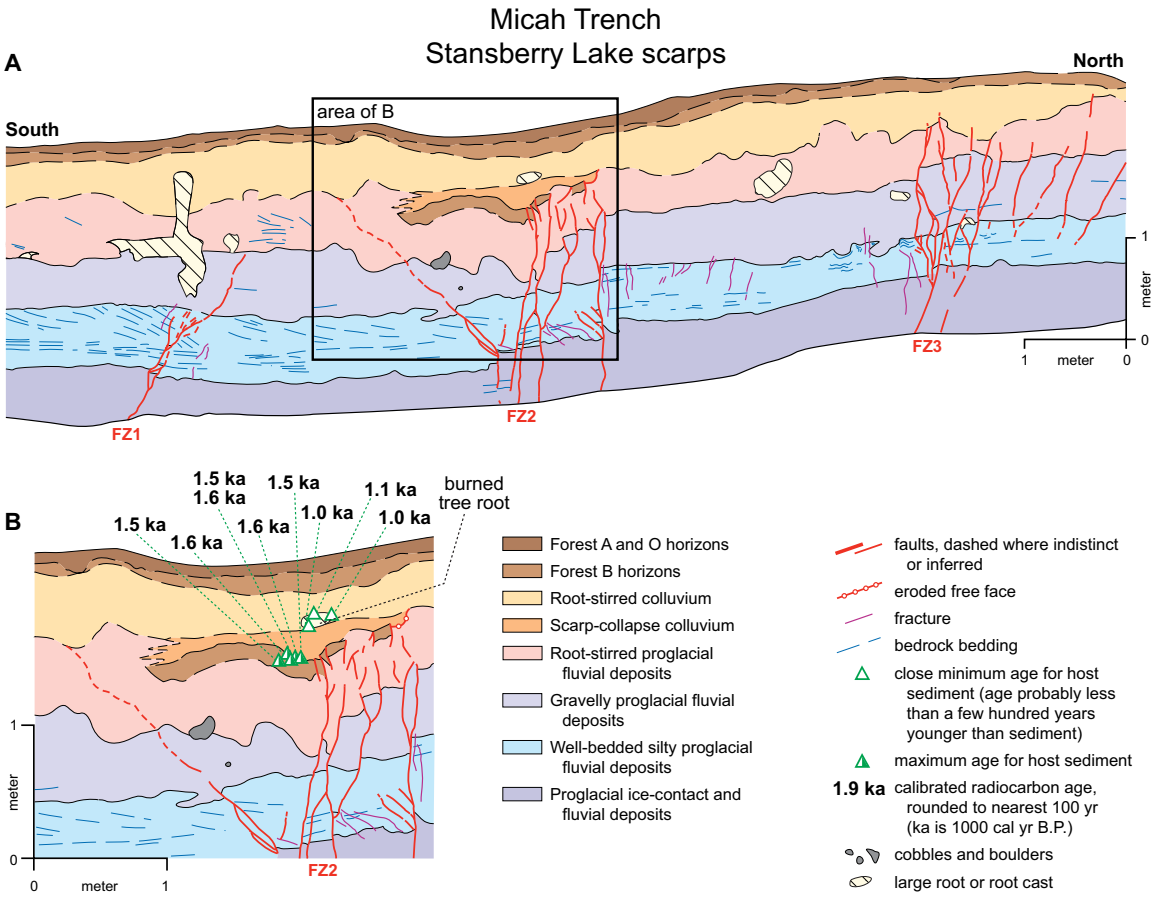

C Sequence of events

1 Deposition of proglacial ice-contact and fluvial deposits in the vicinity of the Puget glacial lobe (probably 17–16 ka).

2 Deposition of silty to gravelly proglacial fluvial deposits (probably 17–15 ka).

3 Development of a forest soil with a structural B horizon on the proglacial fluvial deposits, followed by extensive root stirring (postglacial through late Holocene).

4 Oblique-slip faulting at a 60° angle to the trend of the Tacoma fault zone with an unknown ratio of vertical to right-lateral slip (0.6 m vertical displacement across the three fault zones) after 1530–1400 cal yr B.P. and shortly before 1060–960 cal yr B.P.

5 Erosion of the 0.4-m-high fault scarp in fault zone 2 and deposition of a wedge of proximal scarp-derived colluvium over the B horizon adjacent to the scarp.

6 Continued forest soil development with root stirring on the hanging wall and footwall of the scarp and development of a weak forest soil overlying the scarp colluvial wedge.

7 Growth of a tree root in the developing soil near the top of the colluvial wedge, followed by a forest fire during which most of the exterior of the root burned.

8 Continued forest soil development with root stirring on the hanging wall and footwall of the scarp and development of a weak soil overlying the scarp colluvial wedge.

Figure 13. Fault scarp stratigraphy, ages, and interpretation for the Micah trench, Stansberry Lake scarps, hanging wall of Tacoma fault (Figs. 1C and 2B). (A) Central two-thirds of northwest wall of Micah trench (m5 to m16 on trench wall grid of Nelson et al., 2008, http://pubs.er.usgs.gov/usgspubs/sim/sim3060). Faults zones are labeled FZ1, FZ2, and FZ3. (B) Close-up of stratigraphy and faults in FZ2 of the Micah trench. (C) Sequence of depositional and faulting events in the trench. Steve Personius, Gary Henley II, Alan Nelson, Liz Shermer, Eliza Nemser, Trenton Cladouhos, and Lee-Ann Bradley described, sampled, and interpreted the trench.

et al., 2004a). The interval (1050–980 cal yr B.P.) closely overlaps the wiggle-matched age for a drowned stump inferred to record coseismic subsidence at Red Salmon Creek (1090–1010 cal yr B.P.; Sherrod, 2001) as well as the time of the Restoration Point earthquake (1050–1020 cal yr B.P.).

LATE HOLOCENE EARTHQUAKES ELSEWHERE IN THE SOUTHERN PUGET LOWLAND

Recent magnetic, structural, and paleoseismic studies conclude that faults of the Saddle Mountain deformation zone record north-directed uplift of the Seattle uplift area during the Holocene (Fig. 1C; Witter et al., 2008; Blakely et al., 2009; Lamb et al., 2009; Polenz et al., 2010, 2011, fig. 8 therein). Early investigations of the Saddle Mountain deformation zone showed late Holocene slip on the Saddle Mountain East fault and ponding of a swamp against the fault scarp

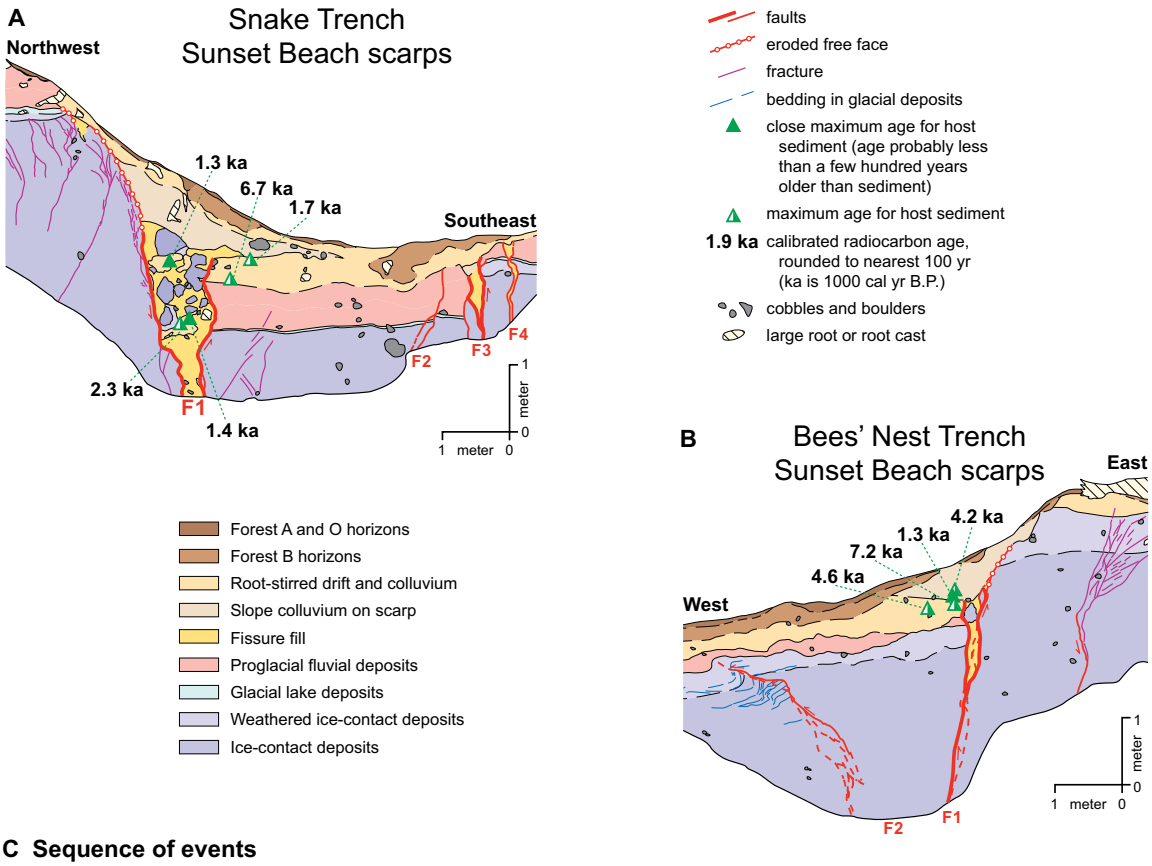

C Sequence of events

1 Deposition of subglacial ice-contact deposits by the Puget glacial lobe shortly followed by deposition of silty sediment in a subglacial or proglacial lake (probably 17–16 ka).
2 Deposition of subglacial and/or proglacial ice-contact and fluvial deposits (probably 17–15 ka).
3 Development of a forest soil with a structural B horizon on the ice-contact and fluvial deposits, followed by extensive root stirring (postglacial through late Holocene).
4 Normal faulting with displacement of 2.4 m (4 m total displacement including antithetic faulting on F2, F3, and F4) on the northwest edge of the graben and 1.8 m of displacement on the southeast edge after 1290–1080 cal yr B.P. (youngest age from each trench; Table S1).
5 Erosion of fault scarps and deposition of wedges of proximal scarp-derived colluvium adjacent to scarps.
6 Continued forest soil development with root stirring on the hanging wall and footwall of the scarps and development of a forest soil on the slope colluvium overlying the scarp colluvial wedges.

Figure 14. Fault scarp stratigraphy, ages, and interpretation for the Snake and Bees' Nest trenches, Sunset Beach scarps, Tacoma fault zone (Figs. 1C and 2B). (A) Central two-thirds of southwest wall of Snake trench (m9 to m1 on trench wall grid of Nelson et al., 2008, http://pubs.er.usgs.gov/usgspubs/sim/sim3060). Ice-contact deposits have been faulted down to the southeast along a normal fault (F1) on the northwest edge of a 60-m-wide, northeast-trending graben on the hanging wall of the Tacoma fault. Faults F2, F3, and F4 are small faults antithetic to fault F1. (B) Central three-quarters of the north wall of Bees' Nest trench (m2 to m9 on trench wall grid of Nelson et al., 2008). Ice-contact deposits have been faulted down to the northwest along a normal fault (F1) on the opposite side (southeast) of the graben in A. Fault F2 is a small fault antithetic to fault F1. (C) Sequence of depositional and faulting events in the Snake and Bees' Nest trenches. Steve Personius, Rob Witter, Harvey Kelsey, Jason Buck, Rich Koehler, Alan Nelson, and Lee-Ann Bradley described, sample, and interpreted the Snake trench. Alan Nelson, Rich Koehler, Rob Witter, Steve Personius, Harvey Kelsey, Lee-Ann Bradley, and Jason Buck described, sampled, and interpreted the Bees' Nest trench.

(Fig. 1C; Carson, 1973; Wilson et al., 1979; Table 1; Table S1 in the Supplemental File [see footnote 1]). Recently, Barnett et al. (2009) and Czajkowski et al. (2009) identified multiple late Holocene faulting events on a fault east of the Saddle Mountain East fault, and Witter et al. (2008) dated two surface-rupturing earthquakes to 17–7.7 ka and after 1.7 ka on a parallel fault to the west, the Saddle Mountain West fault (Fig. 1C). As noted by Jacoby et al. (1992), stumps killed by earthquake-induced flooding in Price Lake and nearby wetlands between the faults near Saddle Mountain give close maximum ages for the most recent movement on the faults (Blakely et al., 2009; Polenz et al., 2011; Table 1). Hughes (2005) used ^{14}C ages on cones and needles from Price Lake and counts of rings from submerged stumps to limit the time of this earthquake to 1300–1000 cal yr B.P.. Preliminary correlations of tree rings date stumps killed by flooding as a result of surface rupture

on Saddle Mountain faults to ~1300–1200 cal yr B.P. (Snook, 2011). Normal fault displacement (2.5 m) on the Frigid Creek scarps, south of the Saddle Mountain faults, was dated by Blakely et al. (2009) to 5.6–0.3 ka (Fig. 1C; Table S1 in the Supplemental File [see footnote 1]).

In the Cargill Creek trench on the Saddle Mountain West fault, Witter et al. (2008) inferred that the younger of two charcoal samples in colluvium deposited after the most recent faulting probably postdated the faulting. Following this inference, we used the youngest maximum age from a drowned stump in Price Lake (Wilson et al., 1979; Hughes, 2005; Polenz et al., 2011, Appendix A therein) with this youngest charcoal age as a minimum age (ages of 1270–930 cal yr B.P. and 1170–940 cal yr B.P.; Table 1), to calculate an OxCal modeled probability distribution for the time of the most recent earthquake or earthquakes on the Saddle Mountain West fault (Fig. 5). For the Saddle Mountain East fault, we used the three youngest maximum ages from Price Lake to calculate a skewed probability distribution for its most recent earthquake, as we did for earthquake E in the Seattle fault zone. Both distributions overlap the time of the millennial earthquake series.

To the southeast at the bend in Hood Canal, cores and exposures on the Skokomish River delta reveal the sudden conversion of a tide flat to a forest due to uplift ~1100 yr ago (Fig. 1C; Martin, 2011). Probable folding of the Skokomish River floodplain above a blind fault may date from about the same time (Polenz et al., 2010). The oblique, left-lateral Canyon River fault, 27 km to the west of the Skokomish River (Fig. 1C), also slipped <2000 yr ago (Fig. 1B; Walsh and Logan, 2007; Polenz et al., 2011).

Terrestrial landslides likely induced by strong shaking, particularly those that dammed stream valleys to form lakes, have been dated in Lake Sammamish near the eastern end of the Seattle fault zone (Fig. 1C), in the Cascade Mountains north and south of Puget Sound, and in the southeast Olympic Mountains (Logan et al., 1998; Pringle et al., 1998). Ages for submerged stumps in Lake Sammamish and four lakes in the Olympic Mountains suggest that lake dams may have coincided with the millennial earthquake series (Schuster et al., 1992; Logan et al., 1998). Other landslides are too imprecisely dated or are too far away from the southern lowland to infer that they record earthquakes in the Seattle or Tacoma fault zones.

DISCUSSION

Diverse rupture modes characterize the earthquake prehistory of the southern Puget Lowland. However, paleoseismology provides firm evidence for the magnitude of only the largest earthquake, named for Restoration Point. As much as 7 m of coseismic uplift at Restoration Point and >2 m of shoreline uplift along at least 40 km of the central Seattle fault zone imply a magnitude of 7–7.5 for this earthquake (Bucknam et al., 1992; Sherrod et al., 2000; ten Brink et al., 2006; Kelsey et al., 2008). Widespread tsunami, liquefaction, and landslide deposits are consistent with an earthquake of this size (Atwater and Moore, 1992; Blakely et al., 2009; Arcos, 2012; Martin and Bourgeois, 2012). At sites that record thousands of years of relatively continuous sedimentation, evidence attributed to the Restoration Point earthquake is more distinct and/or suggests greater deformation or stronger shaking than evidence for any other earthquake (Sherrod et al., 2000; Nelson et al., 2003a; Karlin et al., 2004; Kelsey et al., 2008).

Surface deformation during several historical earthquakes near M 7 on forearc and intraplate thrust faults is broadly analogous to that inferred for the central Seattle fault zone. Uplift of as much as 2.7 m in the Hikurangi forearc of New Zealand during the 1931 M_w7.8 Hawke's Bay earthquake extended over an area ~100 km long and as much as 20 km wide (Hull, 1990). Marine terrace uplift of 1–4 m during 7 prehistoric earthquakes on thrusts in the same region is inferred to record earthquakes of M 7–7.5 (Berryman et al., 2011). Surface ruptures during the 1896 M 7.2 Riku-u earthquake in Japan showed a maximum vertical displacement of 3.5 m along four fault segments (37 km total length), and vertical displacement due to rupture of 4 main fault segments (40 km) during the 1980 M_w6.7 El Asnam, Algeria, earthquake reached 5 m (Rubin, 1996; Wesnousky, 2008). Even the greatest vertical displacements measured across scarps of the largest continental thrust earthquakes (Kaneda et al., 2008a; Xu et al., 2009) do not exceed the uplift measured for the Seattle fault at Restoration Point. These and other historical earthquakes on forearc and intraplate thrusts produced very complex patterns of surface deformation with highly discontinuous fold and fault scarps of variable height and orientation on multiple fault segments (Philip et al., 1992; Rubin, 1996; Kelsey et al., 1998; McCalpin and Carver, 2009).

Widespread evidence for other large to very large Holocene earthquakes in the southern lowland is limited to the millennial series, and the number of earthquakes remains unclear. The spatial extent of evidence for uplift and subsidence (>600 km^2) and the >1 m of deformation at 15 sites in the Tacoma fault zone imply a large earthquake or earthquakes within the millennial earthquake series (Fig. 1C; Bucknam et al., 1992; Sherrod, 2001; Sherrod et al., 2004a; Arcos, 2012). If, as assumed in our OxCal analysis of Tacoma fault zones ages (Fig. 5), this deformation was the result of a large to very large earthquake (Sherrod et al., 2004a; Smith and Karlin, 2009), empirical magnitude-rupture area relations suggest that its magnitude was near 7.0 (Wells and Coppersmith, 1994). Because empirical relations for thrust faults are based on a small number of earthquakes with complex, variable rupture patterns, such empirical-relation estimates of magnitude are more uncertain than those for normal or strike-slip faults (Wesnousky, 2008; McCalpin, 2009).

Two sites with long, relatively continuous records of sedimentation show evidence consistent with earlier large, possibly very large, earthquakes in the central Seattle fault zone. In a small marsh at Restoration Point (Fig. 2A), Sherrod et al. (2000) used transfer function statistical methods on fossil diatom floras from a core to infer that an abrupt change in core lithology reflected a sudden change in tidal environments. They suggested that the change was caused either by coseismic uplift or by the accumulation of a beach bar that partially blocked tidal access to the marsh ca. 7.2–6.4 ka. If coseismic, estimated uplift during this event was 1.5 m compared with at least 7 m during the Restoration Point earthquake. Perhaps the 1.5 m of uplift, comparable to that seen along the Toe Jam Hill fault and Waterman Point fault scarps during earthquakes B, C, or E (Fig. 5; Nelson et al., 2003a), records a rupture of a few kilometers or less on a nearby unmapped fault.

Could the Seattle and Tacoma faults have ruptured during the same very large earthquake, perhaps with a rupture extending westward to faults of the Saddle Mountain deformation zone (Blakely et al., 2009)? Although upper plate structure eastward from the Saddle Mountain deformation zone remains unclear, we hesitate to exclude such a possibility, given some unexpected multifault ruptures of the past approximately two decades (e.g., Sieh et al., 1993; Xu et al., 2009). Earlier historical examples of such ruptures include the en echelon folds >60 km long that grew during the 1586 M~7.7 earthquake on the Yoro blind thrust of central Japan (Ishiyama et al., 2007). Above subduction zone megathrusts, backthrusts tens of kilometers arcward of the megathrust have ruptured during and after great earthquakes (McCalpin and Carver, 2009; Berryman et al., 2011; Wiseman et al., 2011) However, the >20 km distance between the surface projections of the Seattle and Tacoma master-ramp thrusts (Fig. 1C) is greater than the distance between adjacent intraplate faults that have ruptured during the same earthquake (Rubin, 1996; Wesnousky, 2008). How Coulomb stress changes influence the interactions of nearby thrusts depends on many factors in

addition to fault proximity, including fault orientations, prior earthquake timing and magnitudes, and whether thrusts are blind (Stein and Yeats, 1989; Lin and Stein, 2004; Ishiyama et al., 2007; Schwartz et al., 2012). Rupture modeling of thrust faults (e.g., Wang and Chen, 2001; Lin and Stein, 2004), and of central Seattle fault deformation during the Restoration Point earthquake (ten Brink et al., 2006), do not directly address simultaneous rupture on thrusts so far apart. A likely rupture scenario is that upper plate stress changes induced by the Restoration Point earthquake on the master-ramp thrust of the Seattle fault triggered slip on adjacent, updip parts of the fault, and perhaps faults of the Tacoma fault zone or Saddle Mountain deformation zone, days to decades after the earthquake (Sherrod, 2001; Sherrod et al., 2004a; Johanson and Bürgmann, 2010; Schwartz et al., 2012). A possible analogous earthquake series is the sequence of four M_w5.8–6.7 thrust earthquakes in the central California Coast Ranges during 1982–1985 that may have been partially triggered by stress changes induced by the 1857 M_w7.9 Fort Tejon earthquake on the San Andreas fault (Lin and Stein, 2004).

Evidence for the magnitude of other Puget Lowland earthquakes during the late Holocene is ambiguous for two reasons: (1) the evidence is spatially more limited than that for the largest earthquakes during the millennial earthquake series, and (2) the typically >50 yr errors on earthquake ages prevent use of routine ^{14}C dating for site-to-site correlation of closely spaced earthquakes. Paleoseismic studies in a variety of tectonic settings face similar correlation uncertainties (Burbank and Anderson, 2001; Atwater et al., 2004; McCalpin, 2009; e.g., Fraser et al., 2010; DuRoss et al., 2011; Berryman et al., 2012). For example, in a study of scarp geomorphology and stratigraphy in the Hikurangi forearc, Kelsey et al. (1998) concluded that trench stratigraphy could not distinguish among prehistoric ruptures postulated to extend 15, 25, 34, or possibly 130 km along the Poukawa fault zone. In the Seattle fault zone, measured amounts of surface deformation for these other earthquakes are smaller than for deformation that we correlate with the Restoration Point earthquake, suggesting earthquakes of smaller magnitude. Whether these earthquakes were large (M 6.5–7.0) or moderate (M 6.0–6.5), however, depends on which of several fault zone models best applies (Fig. 3). Until structural relations among backthrusts and master-ramp thrusts are clarified, paleoseismic evidence cannot discriminate large from moderate prehistoric earthquakes in the Seattle fault zone.

Limited evidence from the Tacoma fault zone is equally ambiguous about rupture modes, although some evidence suggests multiple earthquakes. For example, Sherrod (2001) ascribed the burial of a marsh soil at Wollochet Bay (Fig. 1C) to subsidence during an earthquake younger than the Restoration Point earthquake. Preliminary tree-ring correlations date stumps killed by flooding, a result of surface rupture on the Saddle Mountain faults, to >50 yr before the Restoration Point earthquake (Hughes, 2005; Snook, 2011). At heights as great as 7–8 m, the Catfish lake scarps within the Tacoma fault zone are too high to have formed entirely during a single large earthquake (e.g., Ishiyama et al., 2007), and the 6-m-high scarp at 1 site (Cedars trench, Nelson et al., 2008, sheet 3) is younger than 4.3 ka (Figs. 1C and 2B; Table 1; Fig. S6 in the Supplemental File [see footnote 1]).

Two consequences of forearc structure that the Puget Lowland shares with intraplate thrust fault systems cloud estimates of the frequency and degree of clustering of large earthquakes in the lowland: uncertain structural relations among faults and probable blind thrusting. Evidence from 2 short backthrusts in the central Seattle fault zone records a cluster of at least 4 late Holocene earthquakes after 2.7 ka. Earthquakes B and C occurred before and earthquake E occurred after the Restoration Point earthquake (which we correlate with earthquake D), and are separated from prior or subsequent earthquakes by intervals of 100–1500 yr (Fig. 5). Records of wetland sedimentation from these sites make it unlikely that similar earthquakes occurred in the preceding 6000–8000 yr and perhaps not since 15 ka (Nelson et al., 2003a; Figs. 10 and 11). However, because the structural relations of these scarps with the master-ramp thrust of the Seattle fault remain uncertain, we cannot determine to what extent the cluster represents the earthquake history of the master Seattle thrust. The same uncertainties afflict the early and middle Holocene earthquake history of the Tacoma fault, where well-dated earthquake evidence is limited to the millennial earthquake series. An additional complication is that most historical earthquakes on forearc and intraplate thrusts have involved rupture of some shallow secondary faults but not others (McCalpin and Carver, 2009; Philip and Meghraoui, 1983; Hull, 1990; Xu et al., 2009). As inferred by Kelsey et al. (1998) from trenches at three sites on faults of the Poukawa fault zone in the Hirugani forearc, our mapping of trenches in the Seattle fault zone shows that not every late Holocene scarp ruptured during each surface-deforming earthquake.

Because blind or almost blind thrusting is ubiquitous in forearc and intraplate thrust systems, an absence of evidence for surface deformation during Holocene earthquakes in the lowland does not imply an absence of earthquakes. A common theme is that even for well-studied modern earthquakes with tens to hundreds of kilometers of complex fault and fold scarps (e.g., 1988 M_s7 Spitak, Armenia; 2008 M_w7.9 Wenchuan, China), some slip on blind thrusts must be invoked to fully explain patterns of surface deformation (e.g., Hull, 1990; Rubin, 1996; Ishiyama et al., 2007; de Michele et al., 2010). Slip on blind thrusts during earthquakes as large as M_w7.7 has produced too little surface evidence of deformation to be preserved for more than decades (e.g., McCalpin and Thakkar, 2003). More commonly, slip on buried thrusts creates small, discontinuous fold or fault scarps that are so eroded or buried within 50–200 yr that surface evidence of them can no longer be identified (Lettis et al., 1997; McCalpin and Carver, 2009).

However, blind thrusting during successive earthquakes may create subtle, long-wavelength folds that warp marine or fluvial terraces (Burbank and Anderson, 2001; e.g., Philip and Meghraoui, 1983; Scharer et al., 2006; Ishiyama et al., 2007; Kaneda et al., 2008b). Substantial blind thrusting is inferred from evidence of this type along an 8-km-long reach of Big Beef Creek, at the western end of the Seattle uplift about half-way between the surface ruptures at Waterman Point and Saddle Mountain (Fig. 1C). There, recessional glaciofluvial terraces crossing the Seattle fault have been arched upward 23 m since 16 ka (Tabor et al., 2011). The uplift has occurred along a stretch of the fault with no discernible surface rupture, implying either large Restoration Point–style earthquakes or many smaller earthquakes on a blind, south-dipping thrust.

Can records of strong shaking over many thousands of years, such as the Karlin et al. (2004) turbidite history from Lake Washington, help distinguish differing rupture modes or earthquake clustering in the lowland? Karlin and Abella (1996) inferred as many as 21 magnetic susceptibility peaks in Lake Washington cores to mark turbidites that record strong earthquake shaking since 7.6 ka, for an average turbidite recurrence of 300–400 yr. Based on uniform sedimentation rates controlled by the 47 ^{14}C ages of Karlin and Abella (1996; see Karlin et al., 2004), some of the turbidites recur every 100–300 yr for periods lasting a thousand years. A large peak that could record strong shaking from a large, regional earthquake occurs in all cores ca. 7.4 ka, but at least 4 younger peaks are larger and whether all such peaks record earthquake shaking is uncertain (Karlin and Abella, 1996; Karlin et al., 2004). Conversely, all earthquakes that strongly shook the lowland are not necessarily recorded by Lake Washington turbidites, and some turbidites may have

been triggered by earthquakes that left no evidence of surface deformation. The lake's late Holocene record shows age distributions for shaking-induced turbidites that span the times of as few as 3 of the as many as 9 great subduction zone earthquakes of the past 3500 yr (Karlin et al., 2004; Atwater et al., 2004; Nelson et al., 2006; Goldfinger et al., 2012), and the distributions are too wide to infer which turbidites were generated by strong subduction zone shaking. Shaking from deep intraplate earthquakes, such as the M 7.1 earthquake between Tacoma and Olympia in 1949, may have also generated turbidites. Although we infer that lake turbidites record a greater proportion of Seattle fault zone earthquakes than earthquakes in other upper plate fault zones in the Puget Lowland, without estimates of earthquake frequency and magnitude for other fault zones, the proportions of turbidite-marked earthquakes they produced are unknown. Such uncertainty in the interpretation of earthquake sources is a major issue in studies of shaking-induced deposits in lakes adjacent to Holocene faults (Goldfinger, 2009; e.g., Inouchi et al., 1996; Ken-Tor et al., 2001; Strasser et al., 2013).

Hazard assessment in the Puget Lowland benefits from the additional information our reconstruction of earthquake history provides. The history increases the minimum number of closely spaced, surface-rupturing earthquakes in the central Seattle fault zone from 3 to 4, shows that the most recent of these earthquakes postdates the Restoration Point earthquake, and confirms on a second backthrust scarp the inference of Nelson et al. (2003a) that the cluster of late Holocene earthquakes followed a period of ~6000–8000 yr of scarp quiescence. The history suggests that faults of the central Seattle fault zone may slip during moderate to large earthquakes as frequently as every few hundred years for periods of ~1000–2000 yr, and then not slip for periods of at least several thousands of years. Our dating narrows the time interval for the millennial earthquake series, particularly in the Tacoma fault zone, but cannot address the prospect of simultaneous rupture of two or more fault zones in the southern lowland. Despite the uncertainties in actual earthquake history, hazard assessment methods accommodate the diverse rupture modes inferred from the findings described here through weighting of alternative rupture models with a range of probabilities (e.g., Petersen et al., 2008).

CONCLUSIONS

Our evaluation of new and previously published paleoseismic data improves the understanding of the earthquake prehistory of the southern Puget Lowland, and illustrates some limitations of using paleoseismic data to reconstruct earthquake history in forearcs with complex upper plate structure. OxCal analysis of 10 of the most closely limiting ^{14}C ages from fault scarp trenches and cores at 8 sites restrict the age of the M 7–7.5 Restoration Point earthquake in the central Seattle fault zone to 1040–910 cal yr B.P. (2σ; Fig. 5). This age interval overlaps the most precise age for the earthquake's tsunami (1050–1020 cal yr B.P.) in eastern Puget Sound. Limiting ages date stratigraphic evidence for three smaller earthquakes that occurred during time intervals that do not overlap with 1050–1020 cal yr B.P. Two of these, earthquakes B and C, occurred prior to the Restoration Point earthquake, 2650–1940 cal yr B.P. and 1310–1200 cal yr B.P., respectively, and one (earthquake E) occurred after the Restoration Point earthquake between 940 and 380 cal yr B.P. Whether these earthquakes were of moderate (M 5.5–6.0) or large (M 6.5–7.0) magnitude, the surface-deformation history of the central Seattle fault zone suggests that faults may slip during moderate to large earthquakes as frequently as every few hundred years for periods of ~1000–2000 yr, and then not slip for periods of at least several thousands of years.

Despite its value as the potentially most complete and longest record of strong shaking in the Puget Lowland, extracting a history of surface-deforming earthquakes on upper plate faults from Lake Washington's turbidite record is complicated by an abundance of potential earthquakes sources. These include surface-deforming and non-surface-deforming upper plate earthquakes in at least three lowland fault zones (Fig. 1B), Cascadia subduction zone earthquakes, and deep intraplate earthquakes beneath the lowland.

The Tacoma fault zone earthquake history consists of at least one large-magnitude earthquake ca. 1000 cal yr B.P., but evidence is too sparse to determine whether this earthquake was closely predated or postdated by moderate to large earthquakes on faults in the Tacoma basin. Four fault scarp trenches in the Tacoma fault zone described here show the most recent scarp of the Tacoma fault to be late Holocene and date surface rupture on two hanging-wall faults to ca. 1000 cal yr B.P., the time of widespread coseismic subsidence in the Tacoma basin. In the Tacoma fault zone, 12 closely limiting new and previously published ages from 9 sites constrain the earthquake (or a closely spaced series of earthquakes) to 1050–980 cal yr B.P. (Fig. 5). An age from one subsidence site in the Tacoma basin suggests an earthquake slightly younger than this interval. The amount of subsidence measured at another site and the height of the highest fault zone scarps also suggest multiple Holocene earthquakes.

OxCal analysis of previously reported ages for late Holocene earthquakes in the Saddle Mountain deformation zone limit earthquakes on the Saddle Mountain East and Saddle Mountain West faults to 1160–310 cal yr B.P. and 1200–970 cal yr B.P., respectively. Whether these earthquakes were synchronous, with each other or possibly with ruptures farther east in the Seattle fault zone or Tacoma fault zone, remains unknown.

ACKNOWLEDGMENTS

This work was supported by the Earthquake Hazards Program of the U.S. Geological Survey. Jason Buck, Gary Henley II, Liz Schermer, Koji Okumura, Rob Witter, Rich Koehler, Elizabeth Barnett, Eliza Nemser, Trenton Cladouhos, Ian Madin, Vicky McConnell, and Yoko Ota mapped trenches, collected critical ^{14}C samples or structural data, and helped with interpretation. These and other trench wall mappers are listed in figure captions. Lee Liberty, Bill Stephenson, and many others ran and interpreted geophysical profiles near trenches. We thank many other colleagues for help with trench mapping and for insightful comments during trench reviews. Discussions with Tom Pratt, Kathy Troost, Uri ten Brink, Jonathan Hughes, Rich Briggs, Tim Walsh, Bob Bucknam, and Craig Weaver were particularly helpful. Reviews by Olaf Zielke, Rob Witter, Tom Pratt, Sotiris Kokkalas, and three anonymous reviewers strengthened the paper. Any use of trade, product, or firm names is for descriptive purposes only, and does not imply endorsement by the U.S. Government.

REFERENCES CITED

Arcos, M. E. M., 2012, The A.D. 900–930 Seattle-fault-zone earthquake with a wider coseismic rupture patch and postseismic submergence: Inferences from new sedimentary evidence: Seismological Society of America Bulletin, v. 102, p. 1079–1098, doi:10.1785/0120110123.

Atwater, B.F., 1999, Radiocarbon dating of a Seattle earthquake to A.D. 900–930: Seismological Research Letters, v. 10, p. 232.

Atwater, B.F., and Moore, A.L., 1992, A tsunami about 1,000 years ago in Puget Sound, Washington: Science, v. 258, p. 1614–1617, doi:10.1126/science.258.5088.1614.

Atwater, B.F., Tuttle, M.P., Schweig, E.S., Rubin, C.M., Yamaguchi, D.K., and Hemphill-Haley, E., 2004, Earthquake recurrence inferred from paleoseismology, *in* Gillespie, A.R., et al., eds., The Quaternary Period in the United States: Amsterdam, Elsevier, p. 331–350.

Barnett, E.A., Sherrod, B.L., Kelsey, H.M., Czajkowski, J.L., Walsh, T.J., Contreras, T.A., Davis-Stanton, K., Schermer, E.R., and Carson, R.J., 2009, Active faulting along the Saddle Mountain fault zone, southeast Olympic Mountains, WA: Eos (Transactions, American Geophysical Union), v. 90, Fall Meeting Supplement, abs. S51B–1404.

Barnett, E.A., Haugerud, R.A., Sherrod, B.L., Weaver, C.S., Pratt, T.L., and Blakely, R.J., 2010, Preliminary atlas of active shallow tectonic deformation in the Puget Lowland, Washington: U.S. Geological Survey Open-File Report 2010–1149, 32 p.

Berryman, K., Ota, Y., Miyauchi, T., Hull, A., Clark, K., Ishibashi, K., Iso, N., and Litchfield, N., 2011, Holocene paleoseismic history of upper-plate faults in the southern Hikurangi subduction margin, New Zealand, deduced from marine terrace records: Seismological Society of America Bulletin, v. 101, p. 2064–2087, doi:10.1785/0120100282.

Berryman, K., Cooper, A., Norris, R., Vilamor, P., Sutherland, R., Wright, T., Schermer, E., Langridge, R., and Biasi, G., 2012, Late Holocene rupture history of the Alpine fault in South Westland, New Zealand: Seismological Society of America Bulletin, v. 102, p. 620–638, doi:10.1785/0120110177.

Biasi, G.P., and Weldon, R.J., 2009, San Andreas fault rupture scenarios from multiple paleoseismic records: Stringing pearls: Seismological Society of America Bulletin, v. 99, p. 471–498, doi:10.1785/0120080287.

Bird, M.I., 2007, Radiocarbon dating: charcoal, *in* Elias, S.A., ed., Encyclopedia of Quaternary science: Amsterdam, Elsevier, p. 2950–2958.

Blakely, R.J., Wells, R.E., Weaver, C.S., and Johnson, S.Y., 2002, Location, structure and seismicity of the Seattle fault zone, Washington: Evidence from aeromagnetic anomalies, geologic mapping and seismic reflection data: Geological Society of America Bulletin, v. 114, p. 169–177, doi:10.1130/0016-7606(2002)114<0169:LSASOT>2.0.CO;2.

Blakely, R.J., Sherrod, B.L., Hughes, J.F., Anderson, M.L., Wells, R.E., and Weaver, C.S., 2009, Saddle Mountain fault deformation zone, Olympic Peninsula, Washington: Western boundary of the Seattle uplift: Geosphere, v. 5, p. 105–125, doi:10.1130/GES00196.1.

Bourgeois, J., and Johnson, S.Y., 2001, Geologic evidence of earthquakes at the Snohomish delta, Washington, in the past 1200 yr: Geological Society of America Bulletin, v. 113, p. 482–494, doi:10.1130/0016-7606(2001)113<0482:GEOEAT>2.0.CO;2.

Brocher, T.M., Parsons, T., Blakely, R.J., Christensen, N.I., Fisher, M.A., Wells, R.E., and the SHIPS working group, 2001, Upper crustal structure in Puget Lowland, Washington: Results from the 1998 seismic hazard investigation in Puget Sound: Journal of Geophysical Research, v. 106, no. B7, p. 13,541–13,564, doi:10.1029/2001JB000154.

Brocher, T.M., Blakely, R.J., and Wells, R.E., 2004, Interpretation of the Seattle uplift, Washington, as a passive roof duplex: Geological Society of America Bulletin, v. 94, p. 1379–1401, doi:10.1785/012003190.

Bronk Ramsey, C., 1995, Radiocarbon calibration and analysis of stratigraphy: The OxCal program: Radiocarbon, v. 37, no. 2, p. 425–430.

Bronk Ramsey, C., 2008, Deposition models for chronological records: Quaternary Science Reviews, v. 27, p. 42–60, doi:10.1016/j.quascirev.2007.01.019.

Bronk Ramsey, C., 2009, Bayesian analysis of radiocarbon dates: Radiocarbon, v. 51, no. 1, p. 337–360.

Bucknam, R.C., and Biasi, G.P., 1994, An improved estimate of the time of a prehistoric earthquake in the southwest Puget Sound region, Washington: Geological Society of America Abstracts with Programs, v. 26, no. 7, p. A-522.

Bucknam, R.C., Hemphill-Haley, E., and Leopold, E.B., 1992, Abrupt uplift within the past 1,700 years at southern Puget Sound, Washington: Science, v. 258, no. 5088, p. 1611–1614, doi:10.1126/science.258.5088.1611.

Bucknam, R.C., Sherrod, B.L., and Elfendahl, G.W., 1999, A fault scarp of probable Holocene age in the Seattle fault zone, Bainbridge Island, Washington: Seismological Research Letters, v. 258, p. 1611–1614.

Burbank, D.W., and Anderson, R.S., 2001, Tectonic geomorphology: Oxford, U.K., Blackwell Publishing, 274 p.

Carson, R.J., 1973, First known active fault in Washington: Washington Division of Geology and Earth Resources, Washington Geologic Newsletter, v. 1, no. 3, p. 1–2.

Chang, S.E., 2010, Urban disaster recovery: A measurement framework and its application to the 1995 Kobe earthquake: Disasters, v. 34, p. 303–327, doi:10.1111/j.1467-7717.2009.01130.x.

Clement, C.R., Pratt, T.L., Holmes, M.L., and Sherrod, B.L., 2010, High-resolution seismic reflection imaging of growth folding and shallow faults beneath the southern Puget Lowland, Washington State: Seismological Society of America Bulletin, v. 100, p. 1710–1723, doi:10.1785/0120080306.

Czajkowski, J.L., Walsh, T.J., Contreras, T.A., Davis-Stanton, K., Kelsey, H.M., Schermer, E.R., and Carson, R.J., 2009, Active faulting along a newly-found segment of the Saddle Mountain fault zone, southeastern Olympic Mountains, WA—A paleoseismic trenching study: Geological Society of America Abstracts with Programs, v. 41, no. 7, p. 479.

de Michele, M., Raucoules, D., de Sigoyer, J., Pubellier, M., and Chamot-Rooke, N., 2010, Three-dimensional surface displacement of the 2008 May 12 Sichuan earthquake, China, derived from synthetic aperture radar: Evidence for rupture on a blind thrust: Geophysical Journal International, v. 183, p. 1097–1103, doi:10.1111/j.1365-246X.2010.04807.x.

DuRoss, C.B., Personius, S.F., Crone, A.J., Olig, S.S., and Lund, W.R., 2011, Integration of paleoseismic data from multiple sites to develop an objective earthquake chronology: Application to the Weber segment of the Wasatch fault zone, Utah: Seismological Society of America Bulletin, v. 101, p. 2765–2781, doi:10.1785/0120110102.

Ekblaw, D., and Leopold, E.B., 1993, Evidence of earthquakes: Late Holocene macrofossil sequences and paleoecology of wetlands in Central Puget Sound [abs.]: Missoula, Montana, Pacific Division, American Association for the Advancement of Science Annual Meeting, p. 42.

Finlayson, D.P., 2005, Combined bathymetry and topography of the Puget Lowland, Washington State: University of Washington School of Oceanography, http://www.ocean.washington.edu/data/pugetsound/.

Fraser, J., Hubert-Ferrari, A., Vanneste, K., Altinok, S., and Drab, L., 2010, A relict paleoseismic record of seven earthquakes between 2000 BC and 600 AD on the central North Anatolian fault at Elmacik, near Osmancik, Turkey: Geological Society of America Bulletin, v. 122, p. 1830–1845, doi:10.1130/B30081.1.

Fumal, T.E., Rymer, M.J., and Seitz, G.G., 2002, Timing of large earthquakes since AD 800 on the Mission Creek strand of the San Andreas fault zone at Thousand Palms Oasis, near Palm Springs, California: Seismological Society of America Bulletin, v. 92, p. 2841–2860, doi:10.1785/0120000609.

Gavin, D.G., 2001, Estimation of inbuilt age in radiocarbon ages of soil charcoal for fire history studies: Radiocarbon, v. 43, no. 1, p. 27–44.

Goldfinger, C., 2009, Sub-aqueous paleoseismology, *in* McCalpin, J.P., ed., Paleoseismology (second edition): International Geophysics Volume 95: San Diego, California, Academic Press, p. 119–170, doi:10.1016/S0074-6142(09)95050-1.

Goldfinger, C., Nelson, C.H., Morey, A.E., Johnson, J.E., Patton, J.R., Karabanov, E., Gutierrez-Pastor, J., Eriksson, A.T., Patton, J., Gracia, E., Dunhill, G., Enkin, J.R., Dallimore, A., and Vallier, T., 2012, Turbidite event history: Methods and implications for Holocene paleoseismicity of the Cascadia subduction zone: U.S. Geological Survey Professional Paper 1661-F, 332 p.

Harding, D.J., and Berghoff, G.S., 2000, Fault scarp detection beneath dense vegetation cover: Airborne lidar mapping of the Seattle fault zone, Bainbridge Island, Washington State: Proceedings, American Society of Photogrammetry and Remote Sensing Annual Conference, 2000, Washington D.C., p. 1–11.

Harding, D.J., Johnson, S.Y., and Haugerud, R.A., 2002, Folding and rupture of an uplifted Holocene marine platform in the Seattle fault zone, Washington, revealed by airborne laser swath mapping: Geological Society of America Abstracts with Programs, v. 34, no. 5, p. A-107.

Haugerud, R.A., and Harding, D.J., 2001, Some algorithms for virtual deforestation (VDF) of lidar topographic survey data: International Archives of Photogrammetry and Remote Sensing, v. 34, p. 211–217.

Haugerud, R.A., Harding, D.J., Johnson, S.Y., Harless, J.L., and Weaver, C.S., 2003, High-resolution LIDAR topography of the Puget Lowland, Washington—A bonanza for Earth science: GSA Today, v. 13, no. 6, p. 4–10, doi:10.1130/1052-5173(2003)13<0004:HLTOTP>2.0.CO;2.

Hemphill-Haley, E., 1996, Diatoms as an aid in identifying late-Holocene tsunami deposits: The Holocene, v. 6, p. 439–448, doi:10.1177/095968369600600406.

Hughes, J.F., 2005, Meters of synchronous Holocene slip on two strands of a fault in the western Puget Sound Lowland, Washington: Eos (Transactions, American Geophysical Union), v. 90, Fall Meeting Supplement, abs. S51C–1020.

Hull, A.G., 1990, Tectonics of the 1931 Hawke's Bay earthquake: New Zealand Journal of Geology and Geophysics, v. 33, p. 309–320.

Inouchi, Y., Kinugasa, Y., Kumon, F., Nakano, S., Yasumatsu, S., and Shiki, T., 1996, Turbidites as records of intense palaeoearthquakes in Lake Biwa, Japan: Sedimentary Geology, v. 104, p. 117–125, doi:10.1016/0037-0738(95)00124-7.

Ishiyama, T., Mueller, K., Sata, H., and Togo, M., 2007, Coseismic fault-related fold model, growth structure, and the historic multisegment blind thrust earthquake on the basement-involved Yoro thrust, central Japan: Journal of Geophysical Research, v. 112, no. B3, doi:10.1029/2006JB004377.

Jacoby, G.C., Williams, P.L., and Buckley, B.M., 1992, Tree ring correlation between prehistoric landslides and abrupt tectonic events in Seattle, Washington: Science, v. 258, p. 1621–1623, doi:10.1126/science.258.5088.1621.

Johanson, I.A., and Bürgmann, R., 2010, Coseismic and postseismic slip from the 2003 San Simeon earthquake and their effects on backthrust slip and the 2004 Parkfield earthquake: Journal of Geophysical Research, v. 115, no. B7, p. 411, doi:10.1029/2009JB006599.

Johnson, S.Y., Potter, C.J., and Armentrout, J.M., 1994, Origin and evolution of the Seattle fault and Seattle basin, Washington: Geology, v. 22, p. 71–74, doi:10.1130/0091-7613(1994)022<0071:OAEOTS>2.3.CO;2.

Johnson, S.Y., Dadisman, S.V., Childs, J.R., and Stanley, W.D., 1999, Active tectonics of the Seattle fault and central Puget Sound, Washington—Implications for earthquake hazards: Geological Society of America Bulletin, v. 111, p. 1042–1053, doi:10.1130/0016-7606(1999)111<1042:ATOTSF>2.3.CO;2.

Johnson, S.Y., Nelson, A.R., Personius, S.F., Wells, R.E., Kelsey, H.M., Sherrod, B.L., Okumura, K., Koehler, R., III, Witter, R.C., Bradley, L., and Harding, D.J., 2004a, Evidence for late Holocene earthquakes on the Utsalady Point fault, northern Puget Lowland, Washington: Seismological Society of America Bulletin, v. 94, p. 2299–2316, doi:10.1785/0120040050.

Johnson, S.Y., Blakely, R.J., Stephenson, W.J., Dadisman, S.V., and Fisher, M.A., 2004b, Active shortening of the Cascadia forearc and implications for seismic hazards of the Puget Lowland: Tectonics, v. 23, TC1011, doi:10.1029/2003TC001507.

Jovanelly, T.J., and Moore, A.L., 2009, Sedimentological analysis of an ancient sand sheet of multiple origins at Lynch Cove, Puget Sound, Washington: Journal of Coastal Research, v. 25, p. 294–304, doi:10.2112/07-0892.1.

Kaneda, H., Nakata, T., Tsutsumi, H., Kondo, H., Sugito, N., Awata, Y., Akhtar, S.S., Majid, A., Khattak, W., Awan, A.A., Yeats, R.S., Hussain, A., Ashraf, M., Wesnousky, S.G., and Kausar, A.B., 2008a, Surface rupture of the 2005 Kashmir, Pakistan, earthquake and its active tectonic implications: Seismological Society of America Bulletin, v. 98, p. 521–557, doi:10.1785/0120070073.

Kaneda, H., Kinoshita, H., and Komatsubara, T., 2008b, An 18,000-year record of recurrent folding inferred from sediment slices and cores across a blind segment of the Biwako-Seigan fault zone, central Japan: Journal of Geophysical Research, v. 113, B05401, doi:10.1029/2007JB005300.

Karel, P., and Liberty, L.M., 2008, The western extension of the Seattle fault: New insights from seismic reflection data: Eos (Transactions, American Geophysical Union), v. 89, fall meeting supplement, abs. T21B–1951.

Karlin, R.E., and Abella, S.E.B., 1992, Paleoearthquakes in the Puget Sound region recorded in sediments from Lake Washington, U.S.A: Science, v. 258, no. 5088, p. 1617–1620, doi:10.1126/science.258.5088.1617.

Karlin, R.E., and Abella, S.E.B., 1996, A history of Pacific Northwest earthquakes recorded in Holocene sediments from Lake Washington: Journal of Geophysical Research, v. 101, no. B3, p. 6137–6150, doi:10.1029/95JB01626.

Karlin, R.E., Holmes, M., Abella, S.E.B., and Sylwester, R., 2004, Holocene landslides and a 3500-year record of Pacific Northwest earthquakes from sediments in Lake

Washington: Geological Society of America Bulletin, v. 116, p. 94–108, doi:10.1130/B25158.1.

Kelsey, H.M., Hull, A.G., Cashman, S.M., Berryman, K.R., Cashman, P.H., Trexler, J.H., Jr., and Begg, J.G., 1998, Paleoseismology of an active reverse fault in a forearc setting: The Poukawa fault zone, Hikurangi forearc, New Zealand: Geological Society of America Bulletin, v. 110, p. 1123–1148, doi:10.1130/0016-7606(1998)110<1123:POAARF>2.3.CO;2.

Kelsey, H.M., Sherrod, B.L., Nelson, A.R., and Brocher, T.M., 2008, Earthquakes generated from bedding-plane-parallel reverse faults above an active wedge thrust, Seattle fault zone: Geological Society of America Bulletin, v. 120, p. 1581–1597, doi:10.1130/B26282.1.

Kelsey, H.M., Sherrod, B.L., Blakely, R.J., and Haugerud, R.A., 2012, Holocene faulting in the Bellingham forearc basin: Upper-plate deformation at the northern end of the Cascadia subduction zone: Journal of Geophysical Research, v. 117, B03409, doi:10.1029/2011JB008816.

Kemp, A.C., Nelson, A.R., and Horton, B.P., 2013, Radiocarbon dating of plant macrofossils from tidal-marsh sediment, *in* Shroder, J.G., ed., Treatise on geomorphology, Volume 14: San Diego, Academic Press, p. 370–388, doi:10.1016/B978-0-12-374739-6.00400-0.

Ken-Tor, R., Agnon, A., Enzel, Y., Stein, M., Marco, S., and Negendank, J.F.W., 2001, High-resolution geological record of historic earthquakes in the Dead Sea basin: Journal of Geophysical Research, v. 106, no. B2, p. 2221–2234, doi:10.1029/2000JB900313.

Lamb, A.P., Liberty, L.M., Blakely, R.J., and Van Wijk, K., 2009, The Tahuya lineament: Southwestern extension of the Seattle fault?: Geological Society of America Abstracts with Programs, v. 41, no. 7, p. 479.

Lettis, W.R., Wells, D.L., and Baldwin, J.N., 1997, Empirical observations regarding reverse earthquakes, blind thrust faults, and Quaternary deformation: Are blind thrusts truly blind?: Seismological Society of America Bulletin, v. 87, p. 1171–1198.

Liberty, L.M., and Pratt, T.L., 2008, Structure of the eastern Seattle fault zone, Washington State: New insights from seismic reflection data: Seismological Society of America Bulletin, v. 98, p. 1681–1695, doi:10.1785/0120070145.

Lienkaemper, J.J., and Bronk Ramsey, C., 2009, OxCal: Versatile tool for developing paleoearthquake chronologies—A primer: Seismological Research Letters, v. 80, p. 431–434, doi:10.1785/gssrl.80.3.431.

Lienkaemper, J.J., and Williams, P.L., 2007, A record of large earthquakes on the southern Hayward fault for the past 1800 years: Seismological Society of America Bulletin, v. 97, p. 1803–1819, doi:10.1785/0120060258.

Lin, J., and Stein, R.S., 2004, Stress triggering in thrust and subduction earthquakes and stress interaction between the southern San Andreas and nearby thrust and strike-slip faults: Journal of Geophysical Research, v. 109, no. B2, p. 303, doi:10.1029/2003JB002607.

Logan, R.L., and Walsh, T.J., 2007, Geologic map of the Vaughn 7.5-minute quadrangle, Pierce and Mason Counties, Washington: Washington Division of Geology and Earth Resources Geologic Map GM-65, scale 1:24,000, http://www.dnr.wa.gov/Publications/ger_gm65_geol_map_vaughn_24k.pdf.

Logan, R.L., Schuster, R.L., Pringle, P.T., Walsh, T.J., and Palmer, S.P., 1998, Radiocarbon ages of probable coseismic features from the Olympic Peninsula and Lake Sammamish, Washington: Washington Geology, v. 26, no. 2–3, p. 59–67.

Lukac, M., and Godbold, D.L., 2011, Soil ecology in northern forests: A belowground view of a changing world: Cambridge, U.K., Cambridge University Press, 268 p.

Martin, M.E., 2011, Coastal marsh stratigraphy as an indicator of past earthquakes, Puget Lowland, Washington State [Ph.D. thesis]: Seattle, University of Washington, 186 p.

Martin, M.E., and Bourgeois, J., 2012, Vented sediments and tsunami deposits in the Puget Lowland, Washington—Differentiating sedimentary processes: Sedimentology, v. 59, p. 419–444, doi:10.1111/j.1365-3091.2011.01259.x.

McCaffrey, R.A., Qamar, A.I., King, R.W., Wells, R.E., Khazaradze, G., Williams, C.A., Stevens, C.W., Vollick, J.J., and Zwick, P.C., 2007, Fault locking, block rotation and crustal deformation in the Pacific Northwest: Geophysical Journal International, v. 169, p. 1315–1340, doi:10.1111/j.1365-246X.2007.03371.x.

McCalpin, J.P., 2009, Application of paleoseismic data to seismic hazard assessment and neotectonic research, *in* McCalpin, J.P., ed., Paleoseismology (second edition): International Geophysics Volume 95: San Diego, California, Academic Press, Chapter 9, 106 p., doi:10.1016/S0074-6142(0).

McCalpin, J.P., and Carver, G.A., 2009, Paleoseismology of compressional tectonic environments, *in* McCalpin, J.P., ed., Paleoseismology (second edition): International Geophysics Volume 95: San Diego, California, Academic Press, p. 315–419, doi:10.1016/S0074-6142(09)95005-7.

McCalpin, J.P., and Thakkar, M.G., 2003, 2001 Bhuj-Kachchh earthquake: Surface faulting and its relation with neotectonics and regional structures, Gujarat, western India: Annals of Geophysics, v. 46, p. 937–956, doi:10.4401/ag-3463.

Nelson, A.R., Johnson, S.Y., Wells, R.E., Pezzopane, S.K., Kelsey, H.M., Sherrod, B.L., Bradley, L., Koehler, R.D., III, Bucknam, R.C., Haugerud, R.A., and Laprade, W.T., 2002, Field and laboratory data from an earthquake history study of the Toe Jam Hill fault, Bainbridge Island, Washington: U.S. Geological Survey Open-File Report 02–0060, 22 p., http://pubs.usgs.gov/of/2002/ofr-02-0060/.

Nelson, A.R., Johnson, S.Y., Kelsey, H.M., Wells, R.E., Sherrod, B.L., Pezzopane, S.K., Bradley, L., Koehler, R.D., and Bucknam, R.C., 2003a, Late Holocene earthquakes on the Toe Jam Hill fault, Seattle fault zone, Bainbridge Island, Washington: Geological Society of America Bulletin, v. 115, p. 1388–1403, doi:10.1130/B25262.1.

Nelson, A.R., Johnson, S.Y., Kelsey, H.M., Sherrod, B.L., Wells, R.E., Okumura, K., Bradley, L., Bogar, R., and Personius, S.F., 2003b, Field and laboratory data from an earthquake history study of the Waterman Point fault, Kitsap County, Washington: U.S. Geological Survey Miscellaneous Field Studies Map MF-2423, http://pubs.usgs.gov/mf/2003/mf-2423/.

Nelson, A.R., Johnson, S.Y., Kelsey, H.M., Sherrod, B.L., Wells, R.E., Personius, S.F., Okumura, K., Bradley, L., and Bogar, R., 2003c, Late Holocene earthquakes on the Waterman Point reverse fault, another ALSM-discovered fault scarp in the Seattle fault zone, Puget lowland, Washington: Geological Society of America Abstracts with Programs, v. 35, no. 6, p. 98.

Nelson, A.R., Kelsey, H.M., and Witter, R.C., 2006, Great earthquakes of variable magnitude at the Cascadia subduction zone: Quaternary Research, v. 65, p. 354–365, doi:10.1016/j.yqres.2006.02.009.

Nelson, A.R., Personius, S.F., Buck, J., Bradley, L., Sherrod, B.L., Henley, G., II, Liberty, L.M., Kelsey, H.M., Witter, R.C., Koehler, R.D., III, and Schermer, E.R., 2008, Field and laboratory data from an earthquake history study of scarps in the hanging wall of the Tacoma fault, Mason and Pierce Counties, Washington: U.S. Geological Survey Scientific Investigations Map 3060, http://pubs.er.usgs.gov/usgspubs/sim/sim3060.

Ota, Y., Odagiri, S., Sasaki, H., and Mukoyama, S., 2006, Late Holocene deformation as deduced from the former shoreline height of marine terraces above the Seattle fault zone, Washington State: Seismological Society of Japan Journal, v. 58, p. 385–399.

Petersen, M.D., Frankel, A.D., Harmsen, S.C., Mueller, C.S., Haller, K.M., Wheeler, R.L., Wesson, R.L., Zeng, Y., Boyd, O.S., Perkins, D.M., Luco, N., Field, E.H., Wills, C.J., and Rukstales, K.S., 2008, Documentation for the 2008 update of the United States National Seismic Hazard Maps: U.S. Geological Survey Open-File Report 2008–1128, 61 p.

Philip, H., and Meghraoui, M., 1983, Structural analysis and interpretation of the surface deformations of the El Asnam earthquake of October 10, 1980: Tectonics, v. 2, p. 17–49, doi:10.1029/TC002i001p00017.

Philip, H., Rogozhin, E., Cisternas, A., Bousquet, J.C., Borisov, B., and Karakhanian, A., 1992, The Armenian earthquake of 1988 December 7: Faulting and folding, neotectonics, and paleoseismicity: Geophysical Journal International, v. 110, p. 141–158, doi:10.1111/j.1365-246X.1992.tb00718.x.

Polenz, M., Alldritt, K., Heheman, N.J., Sarikhan, I.Y., and Logan, R.L., 2009, Geologic map of the Belfair 7.5-minute quadrangle, Mason, Kitsap, and Pierce Counties, Washington: Washington Division of Geology and Earth Resources Open File Report 2009–7, scale 1:24,000.

Polenz, M., Contreras, T.A., Czajkowski, J.L., Paulin, G.L., Miller, B.A., Martin, M.E., Walsh, T.J., Logan, R.L., Carson, R.J., Johnson, C.N., Skov, R.H., Mahan, S.A., and Cohan, C.R., 2010, Supplement to geologic maps of the Lilliwaup, Skokomish Valley, and Union 7.5-minute quadrangles, Mason County, Washington—Geologic setting and development around the Great Bend of Hood Canal: Washington Division of Geology and Earth Resources Open File Report 2010–5, 27 p.

Polenz, M., Miller, B.A., Davies, N., Perry, B.B., Hughes, J.F., Clark, K.P., Walsh, T.J., Tepper, J.H., and Carson, R.J., 2011, Analytical data from the Hoodsport 7.5-minute quadrangle, Mason County, Washington, Supplement to Open File Report 2011–3: Washington Division of Geology and Earth Resources, Open File Report 2011–4, 44 p.

Pratt, T.L., and Troost, K.G., 2009, Is downtown Seattle, Washington State, on the hanging wall of the Seattle fault?: Seismological Research Letters, v. 80, p. 376, doi:10.1785/gssrl.80.2.264.

Pratt, T.L., Johnson, S., Potter, C., Stephenson, W., and Finn, C., 1997, Seismic reflection images beneath Puget Sound, western Washington state: The Puget Lowland thrust sheet hypothesis: Journal of Geophysical Research, v. 102, no. B12, p. 27469–27489, doi:10.1029/97JB01830.

Pringle, P.T., Schuster, R.L., and Logan, R.L., 1998, New radiocarbon ages of major landslides in the Cascade Range, Washington: Washington Geology, v. 26, p. 31–39.

Reimer, P.J., Baillie, M.G.L., Bard, E., Bayliss, A., Beck, J.W., Blackwell, P.G., Bronk Ramsey, C., Buck, C.E., Burr, G.S., Edwards, R.L., Friedrich, M., Grootes, P.M., Guilderson, T.P., Hajdas, I., Heaton, T.J., Hogg, A.G., Hughen, K.A., Kaiser, K.F., Kromer, B., McCormac, F.G., Manning, S.W., Reimer, R.W., Richards, D.A., Southon, J.R., Talamo, S., Turney, C.S.M., van der Plicht, J., and Weyhenmeyer, C.E., 2009, IntCal09 and Marine09 radiocarbon age calibration curves, 0–50,000 years cal BP: Radiocarbon, v. 51, p. 1111–1150, doi:10.2458/azu_js_rc.v51i4.3569.

Rubin, C. M., 1996, Systematic underestimation of earthquake magnitudes from large intracontinental reverse faults: Historical ruptures break across segment boundaries: Geology, v. 24, p. 989–992, doi:10.1130/0091-7613(1996) 024<0989:SUOEMF> 2.3.CO;2.

Sarikhan, I.Y., Walsh, T.J., and Cakir, R., 2007, Morphology of the Alderwood landslide; a probable origin for tsunami in Lynch Cove, Puget Sound, Washington: Geological Society of America Abstracts with Programs, v. 39, no. 4, p. 31.

Scharer, K.M., Burbank, D.W., Chen, J., and Weldon, R.J., 2006, Kinematic models of fluvial terraces over active detachment folds: Constraints on the growth mechanism of the Kashi-Atushi fold system, Chinese Tian Shan: Geological Society of America Bulletin, v. 118, p. 1006–1021, doi:10.1130/B25835.1.

Schuster, R.L., Logan, R.L., and Pringle, P.T., 1992, Prehistoric rock avalanches in the Olympic Mountains, Washington: Science, v. 258, no. 5088, p. 1620–1621, doi:10.1126/science.258.5088.1620.

Schwartz, D.P., Haeussler, P.J., Seitz, G.G., and Dawson, T.E., 2012, Why the 2002 Denali fault rupture propagated onto the Totschunda fault: Implications for fault branching and seismic hazards: Journal of Geophysical Research, v. 117, no. B11, p. 304, doi:10.1029/2011JB008918.

Sherrod, B.L., 2001, Evidence for earthquake-induced subsidence about 1,100 yr ago in coastal marshes of southern Puget Sound, Washington: Geological Society of America Bulletin, v. 113, p. 1299–1311, doi:10.1130/0016-7606(2001)113<1299:EFEISA>2.0.CO;2.

Sherrod, B.L., 2002, Late Quaternary surface rupture along the Seattle fault zone near Bellevue, Washington: Eos (Transactions, American Geophysical Union), v. 83, fall meeting supplement, abs. S21C–12.

Sherrod, B.L., Bucknam, R.C., and Leopold, E.B., 2000, Holocene relative sea-level changes along the Seattle fault at Restoration Point, Washington: Quaternary Research, v. 54, p. 384–393, doi:10.1006/qres.2000.2180.

Sherrod, B.L., Brocher, T.M., Weaver, C.S., Bucknam, R.C., Blakely, R.J., Kelsey, H.M., Nelson, A.R., and Haugerud, R., 2004a, Holocene fault scarps near Tacoma, Washington, USA: Geology, v. 32, p. 9–12, doi:10.1130/G19914.1.

Sherrod, B.L., Nelson, A.R., Kelsey, H.M., Brocher, T.M., Blakely, R.J., Weaver, C.S., Rountree, N.K., Rhea, B.S., and Jackson, B.S., 2004b, The Catfish Lake scarp, Allyn, Washington: Preliminary field data and implications for earthquake hazards posed by the Tacoma fault: U.S. Geological Survey Open-File Report 2003-455, 14 p., 1 plate, http://pubs.usgs.gov/of/2003/of03-455/.

Sherrod, B.L., Blakely, R.J., Weaver, C.S., Kelsey, H.M., Barnett, E., Liberty, L., Meagher, K.L., and Pape, K., 2008, Finding concealed active faults: Extending the southern Whidbey Island fault across the Puget Lowland, Washington: Journal of Geophysical Research, v. 113, B05313, doi:10.1029/2007JB005060.

Sieh, K., Jones, L., Hauksson, E., Hudnut, K., Eberhart-Phillips, D., Heaton, T., Hough, S., Hutton, K., Kanamori, H., Lilje, A., Lindvall, S., Mcgill, S.F., Mori, J., Rubin, C., Spotila, J.A., Stock, J., Thio, H.K., Treiman, J., Wernicke, B., and Zachariasen, J., 1993, Near-field investigations of the Landers earthquake sequence, April to July 1992: Science, v. 260, no. 5105, p. 171–176, doi:10.1126/science.260.5105.171.

Smith, S., and Karlin, R., 2009, Seismically induced submarine landslides in Puget Sound over the last 1100 years: Geological Society of America Abstracts with Programs, v. 41, no. 7, p. 479–480.

Snook, R., 2011, The use of dendrochronology to establish climate-growth relationships and date a prehistoric earthquake [thesis]: British Columbia, Canada, University of the Fraser Valley, 23 p.

Stein, R.S., and Yeats, R.S., 1989, Hidden earthquakes: Scientific American, v. 260, no. 6, p. 30–39.

Strasser, M., Monecke, K., Schnellmann, M., and Anselmetti, F.S., 2013, Lake sediments as natural seismographs: A compiled record of late Quaternary earthquakes in central Switzerland and its implication for Alpine deformation: Sedimentology, v. 60, no. 1, p. 319–341, doi:10.1111/sed.12003.

Tabor, R., Haugerud, R.A., Haeussler, P.J., and Clark, K.P., 2011, Lidar-revised geologic map of the Wildcat Lake 7.5′ Quadrangle, Kitsap and Mason Counties, Washington: U.S. Geological Survey Scientific Investigations Map SI-3187, scale 1:24,000, 12 p.

Telford, R.J., Heegaard, E., and Birks, H.J.B., 2004, The intercept is a poor estimate of a calibrated radiocarbon age: The Holocene, v. 14, no. 2, p. 296–298, doi:10.1191/0959683604hl707fa.

ten Brink, U.S., Molzer, P.C., Fisher, M.A., Blakely, R.J., Bucknam, R.C., Parsons, T., Crosson, R.S., and Creager, K.C., 2002, Subsurface geometry and evolution of the Seattle fault zone and Seattle basin, Washington: Seismological Society of America Bulletin, v. 92, p. 1737–1753, doi:10.1785/0120010229.

ten Brink, U.S., Song, J., and Bucknam, R.C., 2006, Rupture models for the A.D. 900–930 Seattle fault earthquake from uplifted shorelines: Geology, v. 34, p. 585–588, doi:10.1130/G22173.1.

Walsh, T.J., and Logan, R.L., 2007, Field data for a trench on the Canyon River fault, southeast Olympic Mountains, Washington: Washington Division of Geology and Earth Resources Open File Report 2007–1.

Wang, W.H., and Chen, C.H., 2001, Static stress transferred by the 1999 Chi-Chi, Taiwan, earthquake: Effects on the stability of the surrounding fault systems and aftershock triggering with a 3D fault-slip model: Seismological Society of America Bulletin, v. 91, p. 1041–1052, doi:10.1785/0120000727.

Wells, D.L., and Coppersmith, K.J., 1994, New empirical relationships among magnitude, rupture length, rupture width, rupture area and surface displacement: Seismological Society of America Bulletin, v. 84, p. 974–1002.

Wells, R.E., and Simpson, R.W., 2001, Northward migration of the Cascadia forearc in the northwestern U.S. and implications for subduction deformation: Earth, Planets, and Space, v. 53, p. 275–283.

Wells, R.E., Weaver, C.S., and Blakely, R.J., 1998, Fore-arc migration in Cascadia and its neotectonic significance: Geology, v. 26, p. 759–762, doi:10.1130/0091-7613(1998)026<0759:FAMICA>2.3.CO;2.

Wesnousky, S.G., 2008, Displacement and geometrical characteristics of earthquake surface ruptures: Issues and implications for seismic hazard analysis and the process of earthquake rupture: Seismological Society of America Bulletin, v. 98, p. 1609–1632, doi:10.1785/0120070111.

Whistler, J.E., Atwater, B.F., and Montgomery, D.R., 2002, Holocene liquefaction near the Seattle fault at the Issaquah Creek delta: Eos (Transactions, American Geophysical Union), v. 83, fall meeting supplement, abs. S22B–1036.

Wilson, J.R., Bartholomew, M.J., and Carson, R.J., 1979, Late Quaternary faults and their relationship to tectonism in the Olympic Peninsula, Washington: Geology, v. 7, p. 235–239, doi:10.1130/0091-7613(1979)7<235:LQFATR>2.0.CO;2.

Wiseman, K., Banerjee, P., Sieh, K., Bürgmann, R., and Natawidjaja, D., 2011, Another potential source of destructive earthquakes and tsunami offshore of Sumatra: Geophysical Research Letters, v. 38, no. 10, L10311, doi:10.1029/2011GL047226.

Witter, R.C., Givler, R.W., and Carson, R.J., 2008, Two postglacial earthquakes on the Saddle Mountain West fault, southeastern Olympic Peninsula, Washington: Seismological Society of America Bulletin, v. 98, p. 2894–2917, doi:10.1785/0120080127.

Xu, X., Wen, X., Yu, G., Chen, G., Klinger, Y., Hubbard, J., and Shaw, J., 2009, Coseismic reverse- and oblique-slip surface faulting generated by the 2008 Mw 7.9 Wenchuan earthquake, China: Geology, v. 37, p. 515–518, doi:10.1130/G25462A.1.